Journal of Medicinal Chemistry

pubs.acs.org/jmc

Article

Open Access

This article is licensed under CC-BY 4.0

Potent and Selective Caspase-2 Inhibitors: Biological Profiling, Structural Characterization, and Challenges of Molecular Instability

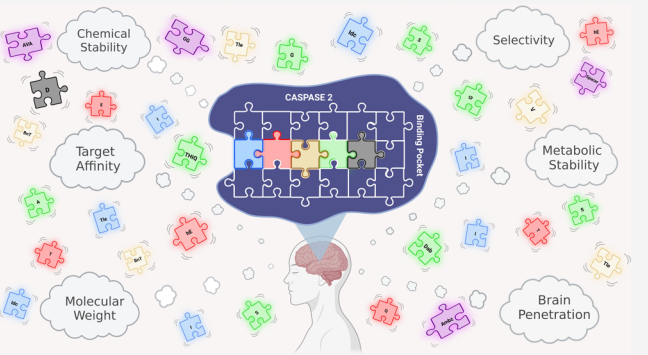
Lisa Forster,[⊥] Bernadette Vallaster,[⊥] Alexander Hubmann, Merlin Bresinsky, Jessica L. Fuller, Ke Shi, Ian P. Lapcinski, Peng Liu, Mu Yang, Jessica M. Strasser, Kathryn M. Nelson, Kristen John, Deepti Mudaliar, Lukas Wirth, Jonas Daschner, Herwig Pongratz, Karen H. Ashe, Michael A. Walters,* and Steffen Pockes*

Cite This: https://doi.org/10.1021/acs.jmedchem.6c01370

Read Online

ACCESS | Metrics & More | Article Recommendations | Supporting Information

ABSTRACT: Caspase-2 (Casp2) has emerged as a promising therapeutic target for neurodegenerative diseases due to its role in pathological tau processing. Here, we designed and synthesized a series of 48 novel peptidomimetic Casp2 inhibitors organized into distinct structural classes. Compounds were evaluated for Casp2 inhibition and selectivity against Casp1, 3, 4, 5, 6, 7, 8, 9, and 10. Inhibitors Idc(hE)G(Dab)D-CHO (**32**) and Idc(hE)G((*S*)-Me-THIQ)D-CHO (**33**) exhibited low nanomolar potency and ≥537-fold selectivity over Casp3. These unprecedented scaffold modifications are consistent with preferred steric arrangements between the P2 and P3 positions. Biochemical assays demonstrated the blockade of tau truncation and impaired the formation of toxic Δtau314. High-resolution crystal structures of compounds **2** and **33** bound to Casp2 revealed binding interactions consistent with the observed SAR. Although Idc(hE)V((*S*)-Me-THIQ)D-CHO (**3**, MUR-65) showed favorable ADME and pharmacokinetic properties, limited membrane permeability, insufficient blood−brain barrier penetration, and P5 indoline instability remain key challenges for further development.



KEYWORDS: *Caspase-2, tau, selectivity, peptidomimetics, covalent reversible inhibitors, Alzheimer's disease*

INTRODUCTION

To date, the available pharmacological interventions for patients with Alzheimer's disease (AD) mainly focus on alleviating the symptoms of the disease instead of fighting the underlying pathological mechanisms.[1] Approved drugs for the symptomatic treatment of AD by the FDA belong to the class of *N*-methyl-*D*-aspartate receptor (NMDAR) antagonists (memantine) or acetylcholinesterase (AchE) inhibitors such as rivastigmine or donepezil.[2] The development of so-called "disease-modifying" therapies that aim to slow down, stop, or even reverse the progression of the disease has largely focused on targeting the *β*-amyloid pathway.[2,3] However, there is an ongoing debate about whether the modest effects of amyloid-clearing antibodies, such as lecanemab, outweigh the risks of serious adverse events.[4,5] Other promising approaches, focusing on the pathology of AD and other tauopathies, are tau-targeting therapies. But to date, none of these tau-targeting drugs have been approved.[6]

In AD, the tau protein undergoes several post-translational modifications that promote aggregation and the formation of neurofibrillary tangles.[7−9] Since the memory deficits and neuronal cell death, which are characteristic of tauopathies, can be dissociated from fibrillar tau,[10] the search for nonfibrillar tau species revealed a 35 kDa tau cleavage product (Δtau314),[11] which has been shown to reversibly impair cognitive and synaptic function in animal and cellular models of tauopathies. Δtau314 is the product of proteolytic cleavage of tau by caspase-2 (Casp2), one of twelve human caspases (cysteine-dependent aspartate-directed proteases) that are involved in processes linked to apoptosis, cell cycle, and inflammation.[11−13] It was shown that mutant tau^{P301L,D314E} that is resistant to Casp2 cleavage prevents tau from excessively accumulating into dendritic spines and impairing synaptic function in mice.[14] Additionally, lowering the Casp2 level in mice with existing deficits restored long-term memory.[11] Further investigations confirmed the presence of Δtau314 proteins in human brains and showed

Received: April 28, 2026
Revised: October 9, 2026
Accepted: October 12, 2026

ACS Publications

© XXXX The Authors. Published by American Chemical Society

Downloaded from pubs.acs.org/jmcmar/article-pdf/doi/10.1021/acs.jmedchem.6c01370/6911434/jm6c01370.pdf by UNIV REGENSBURG user on 17 November 2026

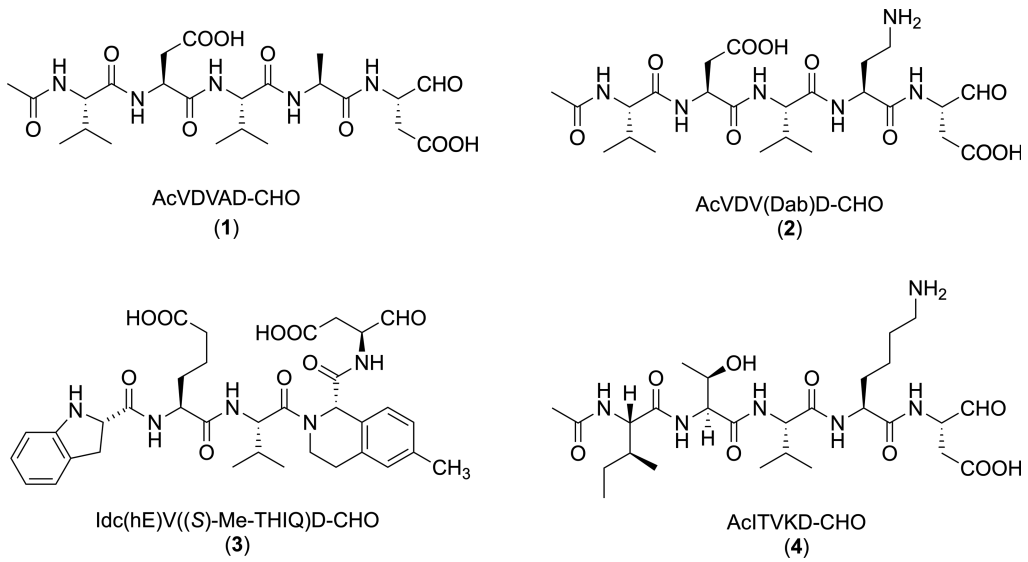


Figure 1. Structures of compounds **1**−**4** that served as the basis for the development of novel Casp2 inhibitors.

elevated levels of Δtau314 and Casp2 in cognitively impaired individuals.[11,15−17] Inhibition of tau truncation by Casp2, therefore, is a promising therapeutic approach for AD and other tauopathies like Huntington's disease (HD) and Lewy body dementia.[11,15−17] On the route to selective Casp2 inhibitors, the strong homology of the active sites of caspases-2 and -3 represents a significant difficulty. By solving the crystal structure of Casp2 and numerous efforts to determine the substrate specificities of the different caspases, some Casp2 preferences for the positions P1−P5 of peptidic substrates/inhibitors could be determined.[18−21] Common for all caspases is the almost absolute preference for aspartic acid at position P1.[22] One crucial structural difference that can be exploited in developing selective Casp2 inhibitors lies in the relative size of the S2 subsite of the substrate binding pocket. In comparison to the other caspases, and especially to caspases-3, -6, and -7, Casp2 can accommodate larger substrates in S2; therefore, sterically demanding P2 residues have been shown to increase Casp2 selectivity.[20,23,24] In contrast, a unique feature of Casp2, compared to the other caspases, is the requirement of at least five amino acids for efficient substrate cleavage.[23] Since Casp2 is a cysteine protease, aldehyde-containing inhibitors act via reversible covalent engagement of the catalytic cysteine residue, forming a transient thiohemiacetal intermediate. Such reversible covalent inhibitors often combine high potency with improved controllability relative to irreversible covalent ligands. Therefore, aldehyde warheads remain a valuable strategy for investigating caspase inhibition and selectivity.

During our previous efforts to expand the knowledge of the structure−activity relationships (SAR) of peptidic inhibitors and Casp2, we synthesized pentapeptidic ligands derived from the canonical inhibitor AcVDVAD-CHO (**1**) (Figure 1). We achieved the highest selectivity in this series by introducing diaminobutyric acid (Dab) at position P2, resulting in the pentapeptide AcVDV(Dab)D-CHO (**2**).[25] Furthermore, we combined structural elements known to promote selectivity and efficacy and partially included non-natural amino acids, as reported by Poreba et al. and Maillard et al..[20,21] We developed the pentapeptide Idc(hE)V((*S*)-Me-THIQ)D-CHO (**3**, MUR-65) (Figure 1), which exhibited a strong inhibitory potency toward Casp2 and significant selectivity over Casp3 (>700-fold)[26] and obtained a crystal structure in complex with JF1cpCasp2.[27] In another approach, we prepared compounds based on peptides representing Casp2 cleavage sequences of endogenous proteins which yielded the pentapeptide AcITVKD-CHO (**4**) (Figure 1). The Ral GTPase-activating protein subunit alpha-1 was used as a model and the aforementioned pentapeptide inhibitor showed moderate inhibitory potency to Casp2 (pK_i = 5.11 ± 0.04 (mean ± SEM, N = 2)) and low selectivity over Casp3 (pK_i = 4.95 ± 0.04 (mean ± SEM, N = 2)).[28] The goal of this study is to improve the physicochemical properties of our compounds by introducing more lipophilic attachments and to investigate the activity and selectivity of these newly developed peptidomimetics. Of particular interest is the selectivity of the molecules over Casp3, which is present in high concentrations in almost all tissues.[29] Selected inhibitors were tested in a caspase panel assay to assess their inhibitory potencies for Casp1-10. We are also interested in improving our inhibitors to be more drug-like according to Lipinski's rule of five[30] or Pfizer's CNS MPO score[31] and exploring different approaches to reduce molecular weight without sacrificing compound activity and selectivity.

Ligand Design

The following section explains the ligand design strategy for the individual subseries in this study and summarizes their structural modifications in a schematic illustration in Figure 2.

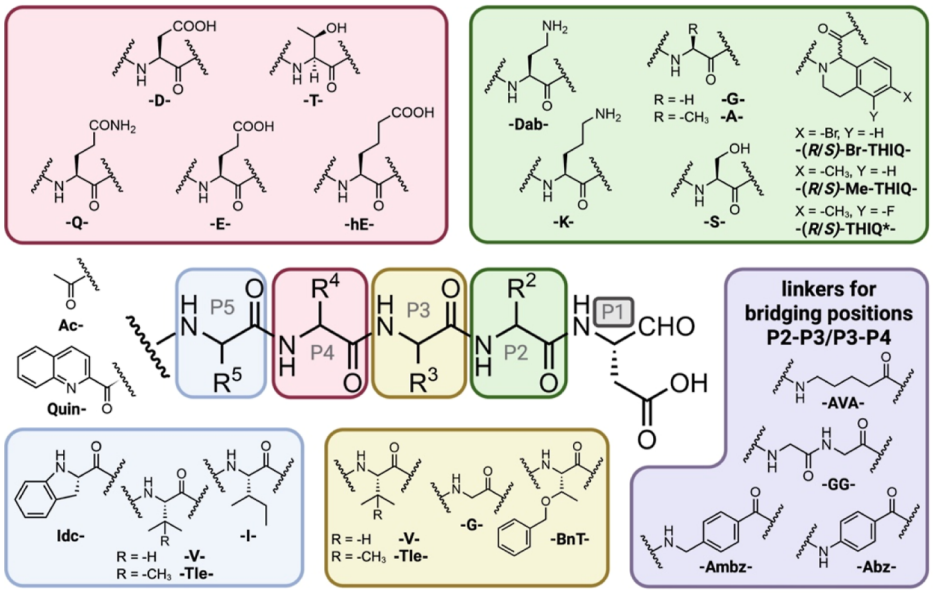
VDVAD Series

We synthesized a series of AcVDVAD-CHO analogs to investigate the introduction of sterically demanding P2 residues and their exchange for smaller substituents. The P2 position has been identified as essential for establishing Casp2 selectivity over other caspases. Among the substrate-binding pockets (S1−S5), the S2 subsite exhibits the most pronounced differences in shape and size across the caspases, with Casp2 possessing the largest S2 pocket.[20,24] This feature can be exploited by incorporating sterically demanding P2 residues, as demonstrated by Maillard et al.,[20] who introduced (un-)substituted tetrahydroisoquinoline (THIQ) residues. In a previously published study, we reported that enantiopure (*S*)-Me-THIQ and 2,4-diaminobutyric acid

Downloaded from pubs.acs.org/jmcmar/article-pdf/doi/10.1021/acs.jmedchem.6c01370/6911434O/jm6c01370.pdf by UNIV REGENSBURG user on 17 November 2026

https://doi.org/10.1021/acs.jmedchem.6c01370
J. Med. Chem. XXXX, XXX, XXX−XXX

A



B

	P5	P4	P3	P2	P1	warhead
VDVAD series						
Ac- Quin-	V Tle Idc	D hE E Q	V Tle G	A S Dab (*R*/*S*)-Br-THIQ (*R*/*S*)-Me-THIQ	D	-CHO
ITVKD series						
Ac-	I	T	V Tle	K (*S*)-Me-THIQ	D	-CHO
Idc series						
	Idc	hE	V Tle G BnT	V G Dab (*S*)-Me-THQ (*S*)-Br-THIQ (*R*/*S*)-Me-THIQ*	D	-CHO
Ac-series						
Ac-	Idc	hE	V Tle G BnT	Dab (*S*)-Me-THIQ	D	-CHO
linker series						
	Idc	hE	-GG- AVA Abz Ambz		D	-CHO
		-GG- AVA		Dab (*S*)-Me-THIQ		

Figure 2. Schematic illustration of the structural modifications applied at positions P2−P5 of the synthesized compounds (panel **A**) and their combinatorial pattern resulting in the five subseries of this study (panel **B**). Chemical structures, short terms, IUPAC names, and synonyms of investigated unnatural amino acids are presented in Table S5 in the Supporting Information. Panel **A** was created with BioRender.com.

(Dab) as P2 substituents are equally effective in mediating Casp2 selectivity. The corresponding pentapeptide inhibitors exhibit high activity, with IC_{50} values in the single- and double-digit nanomolar range.[25,26] Here, we explore the introduction of enantiopure bromine-substituted THIQ or Me-THIQ at the P2 position. Additionally, we investigate the combination with quinaldic acid as a P6 substituent. The quinoline moiety is known to enhance cell membrane permeability and has been incorporated into Casp2 and Casp3 inhibitors that exhibit enhanced pharmacological properties and low in vivo toxicity.[32,33]

Downloaded from pubs.acs.org/jmcmar/article-pdf/doi/10.1021/acs.jmedchem.6c01370/6911434/0/jm6c01370.pdf by UNIV REGENSBURG user on 17 November 2026

https://doi.org/10.1021/acs.jmedchem.6c01370
J. Med. Chem. XXXX, XXX, XXX−XXX

Based on reports that a serine substituent in position P2 is advantageous regarding Casp2 activity,[21] we previously prepared compounds with a P2-serine (AcITVSD-CHO and AcVDVSD-CHO) that exhibited moderate to good Casp2 potency but lacked selectivity (pK_i of 6.01 ± 0.01 (mean ± SEM, $N = 3$) or 7.26 ± 0.06 (mean ± SEM, $N = 3$)).[28] To increase Casp2 selectivity, we synthesized the compound AcV(hE)GSD-CHO (**20**), introducing homoglutamic acid (hE) at the P4 position, due to its proven effectiveness in enhancing Casp2 inhibitory potency and selectivity.[21,26]

To improve the stability of our inhibitors against drug-metabolizing enzymes, we exchanged the P3 and/or P5 valine residues for *L*-α-*tert*-leucine (Tle), a non-natural amino acid commonly found in FDA-approved pharmaceuticals, such as atazanavir or marimastat.[34] It is presumed that the steric hindrance of the additional methyl group in Tle results in enhanced hydrolytic stability.[35]

In a previous investigation, we developed the pentapeptide AcVDV(Dab)D-CHO (**2**), which exhibited promising inhibitory activity ($pK_i = 7.26 \pm 0.07$ (mean ± SEM, $N = 4$)) and showed 28-fold selectivity over Casp3.[25] To further improve this inhibitor, we extended the P4 sidechain by replacing aspartic acid with glutamic acid. To assess the importance of the acidic moiety in position P4, we replaced the glutamic acid with glutamine. Additionally, we modified the canonical Casp2 inhibitor AcVDVAD-CHO by replacing the P5 valine with *S*-indoline-2-carboxylic acid (Idc), an unnatural amino acid, which was reported to be a Casp2 selectivity mediating P5 substituent.[21]

ITVKD Series

Building upon our earlier studies with the pentapeptide AcITVKD-CHO (**4**),[28] we developed inhibitors with individual modifications at the P2 or P3 positions. Specifically, we substituted valine with *tert*-leucine at P3 or introduced (*S*)-Me-THIQ at P2 to investigate the effects on Casp2 selectivity. Furthermore, we shortened the pentapeptide stepwise to tetra- and tripeptides to explore the possibility of reducing the molecular weight while maintaining inhibitory potency and selectivity.

Idc and Ac Series

We previously reported the highly selective pentapeptide Idc(hE)V((*S*)-Me-THIQ)D-CHO (**3**, MUR-65), which exhibited a >794-fold selectivity over Casp3.[26] Based on this early lead structure, we developed a series of penta- and tetrapeptides with structural variations at the P2 and P3 positions. All synthesized inhibitors incorporate Dab, (*S*)-Me-THIQ, or structurally modified THIQ at the P2 position. We found that Casp2 is very tolerant of a broad range of amino acids at position P3, making this position particularly suitable for structural modifications that reduce the molecular weight and potentially optimize physicochemical properties.[25,28] In addition to the above-mentioned exchange of valine to *tert*-leucine, we introduced glycine at P3 and synthesized inhibitors containing a space-occupying O-benzyl-*L*-threonine (BnT), as references. A large-scale peptide library scan identified O-benzyl-L-threonine (BnT) at P3 as particularly beneficial for Casp2 activity,[21] making it valuable for examining structure−activity relationships compared to lower-molecular-weight P3 substituents. All inhibitors of this series share homoglutamic acid (hE) at the P4 position, since this has proven to be advantageous regarding Casp2 inhibitory potency and selectivity. Additionally, throughout this entire series, the unnatural amino acid (*S*)-indoline-2-carboxylic acid (Idc) was incorporated at P5, aligning with prior findings supporting Idc as an effective P5 substituent. Furthermore, it has been stated that Casp2 substrates are stabilized in the enzyme active site through interactions with the *N*-terminal amine group.[21] To assess the impact of *N*-terminal modifications on inhibitory activity, we synthesized inhibitors with both acetylated and non-acetylated Idc residues. For selected acetylated pentapeptide inhibitors, we prepared the respective tetrapeptide analogs lacking the P5 Idc to investigate the influence of peptide length on activity and selectivity.

Linker Series

In another strategy, we attempted to optimize the physicochemical properties and enhance blood−brain barrier (BBB) penetration of our inhibitors. Therefore, we replaced one or two amino acids in the peptide backbone with selected linkers. We developed a series of inhibitors based on Idc(hE)V((*S*)-Me-THIQ)D-CHO or Idc(hE)V(Dab)D-CHO, modified with linkers replacing either the P2−P3 or P3−P4 positions or a single amino acid. We successively inserted spacers such as 5-aminovalerianic acid (AVA), glycine(s), *para*-aminobenzoic (Abz) acid, and *para*-aminomethylbenzoic acid (Ambz) at specific positions along the peptide backbone. We aimed to identify sites in the peptide backbone where linkers are tolerated without the loss of Casp2 inhibitory activity. The selected spacers have comparable lengths (5-aminovalerianic acid: 7.3 Å, glycine−glycine: 7.3 Å, *p*-aminobenzoic acid: 6.3 Å, *p*-aminomethylbenzoic acid 7.4 Å; calculated with Avogadro2[36]) but differ in rigidity, which could influence affinities for Casp2 through altering the arrangement of the inhibitors in the enzyme binding pocket.

Chemistry

The synthesis of peptides **8**−**55** was carried out according to previously described procedures using solid-phase peptide synthesis (SPPS) on an aspartic acid-loaded amino-Merrifield resin in accordance with the standard Fmoc-strategy and is described in the Experimental Section.[25,26,28] Reference compounds **1**−**7** have already been published in earlier studies.[25,26,28] CNS MPO scores of peptides **1**−**55** (Table S1), RP-HPLC stability control of compound **27** and **28** (Figure S1−S4), chemical structures of **1-55** (Figures S7−S61), NMR spectra (Figures S62−S151), RP-HPLC purity controls (Figures S152−S199), and synthesis of the building blocks **BB1**−**BB4** (Scheme S1) are shown in the Supporting Information.

RESULTS AND DISCUSSION

Pharmacology

All synthesized peptides were characterized in a fluorescence-based enzyme inhibition assay regarding their inhibitory potencies for Casp2 and Casp3 (Table 1). Selected inhibitors were additionally investigated in a panel assay for their selectivity over caspases-1, -4, -5, -6, -7, -8, -9, and -10 (Table 2). Throughout this manuscript, Casp2 refers to caspase-2 in general, whereas cpCasp2 denotes the circularly permuted recombinant caspase-2 construct. In contrast to wild-type human Casp2, the mutant cpCasp2 has its large and small subunits swapped and connected by a peptide linker, resulting in a constitutively active single-chain enzyme with higher expression yields in *E. coli* and improved

Downloaded from pubs.acs.org/jmcmar/article-pdf/doi/10.1021/acs.jmedchem.6c01370/6911434/jm6c01370.pdf by UNIV REGENSBURG user on 17 November 2026

https://doi.org/10.1021/acs.jmedchem.6c01370
J. Med. Chem. XXXX, XXX, XXX−XXX

Table 1. Enzyme Inhibitory Potency (pK_i Values) of Peptides 1−55 at cpCasp2 and Casp3[a]

		$pK_i \pm$ SEM				
sequence	cmpd	cpCasp2	N	Casp3	N	K_i (Casp3) / K_i (cpCasp2)
references						
AcVDVAD-CHO	**1**	8.01 ± 0.03	24	8.26 ± 0.07	6	0.3
AcVDV(Dab)D-CHO	**2**	7.26 ± 0.07[b]	4	5.82 ± 0.18[b]	4	28
Idc(hE)V((*S*)-Me-THIQ)D-CHO (MUR-65)	**3**	7.40 ± 0.11[c]	3	< 4.5[c]	3	> 794
AcITVKD-CHO	**4**	6.40 ± 0.16[d]	4	6.05 ± 0.06[d]	4	2
AcDEVD-CHO	**5**	6.60 ± 0.32[b]	3	8.68 ± 0.26[b]	3	0.008
VDVAD series						
AcVDV((*S*)-Me-THIQ)D-CHO	**6**	7.89 ± 0.02[b]	5	6.04 ± 0.06[c]	5	60
AcVDV((*R*)-Me-THIQ)D-CHO	**7**	4.98 ± 0.20[b]	5	< 4.0[c]	4	> 9
AcVDV((*S*)-Br-THIQ)D-CHO	**8**	7.94 ± 0.03	3	6.58 ± 0.02	3	23
AcVDV((*R*)-Br-THIQ)D-CHO	**9**	< 4.8	2	< 4.8	2	1.0
(Quin)VDV((*S*)-Me-THIQ)D-CHO	**10**	7.64 ± 0.09	4	6.49 ± 0.09	4	14
(Quin)VDV((*R*)-Me-THIQ)D-CHO	**11**	5.64 ± 0.31	3	4.94 ± 0.03	3	5.0
(Quin)VDV((*S*)-Br-THIQ)D-CHO	**12**	7.50 ± 0.05	4	6.76 ± 0.03	4	5.5
(Quin)VDV((*R*)-Br-THIQ)D-CHO	**13**	5.37 ± 0.04	3	< 4.8	3	> 3.7
AcVD(Tle)AD-CHO	**14**	7.90 ± 0.09	5	8.18 ± 0.14	6	0.5
Ac(Tle)DVAD-CHO	**15**	7.78 ± 0.08	5	8.17 ± 0.13	6	0.4
Ac(Tle)D(Tle)AD-CHO	**16**	7.84 ± 0.09	5	8.26 ± 0.15	6	0.4
IdcDVAD-CHO	**17**	7.55 ± 0.05	3	8.45 ± 0.10	4	0.1
AcVQV(Dab)D-CHO	**18**	< 4.8	3	< 4.8	3	1.0
AcVEV(Dab)D-CHO	**19**	5.14 ± 0.05	3	< 4.8	3	> 2.2
AcV(hE)GSD-CHO	**20**	7.08 ± 0.04	4	5.72 ± 0.07	4	23
ITVKD series						
AcIT(Tle)KD-CHO	**21**	6.36 ± 0.10	3	6.12 ± 0.09	4	1.7
AcITV((*S*)-Me-THIQ)D-CHO	**22**	6.18 ± 0.06	3	5.11 ± 0.07	4	12
AcTV((*S*)-Me-THIQ)D-CHO	**23**	< 4.8	4	< 4.8	4	1.0
AcV((*S*)-Me-THIQ)D-CHO	**24**	< 4.8	3	< 4.8	4	1.0
Idc series						
Idc(hE)(BnT)(Dab)D-CHO	**25**	7.83 ± 0.07	7	< 4	3	> 6761
Idc(hE)(BnT)((*S*)-Me-THIQ)D-CHO	**26**	6.07 ± 0.08	5	< 4.8	5	> 19
Idc(hE)V(Dab)D-CHO	**27**	7.46 ± 0.04	4	< 4.8	4	> 457
Idc(hE)(Tle)(Dab)D-CHO	**28**	7.09 ± 0.03	4	< 4.8	4	> 195
Idc(hE)(Tle)((*S*)-Me-THIQ)D-CHO	**29**	< 5	3	< 5	3	1.0
Idc(hE)V((*S*)-Me-THIQ*)D-CHO	**30**	7.03 ± 0.09	4	< 5	4	> 107
Idc(hE)V((*R*)-Me-THIQ*)D-CHO	**31**	5.44 ± 0.12	4	< 4.8	3	> 4.4
Idc(hE)G(Dab)D-CHO	**32**	7.72 ± 0.11	11	< 4.8	8	> 832
Idc(hE)G((*S*)-Me-THIQ)D-CHO	**33**	7.95 ± 0.07	9	5.22 ± 0.07	8	537
Idc(hE)VGD-CHO	**34**	7.65 ± 0.07	6	5.17 ± 0.19	4	302
Ac series						
Ac(Idc)(hE)G(Dab)D-CHO	**35**	7.04 ± 0.09	4	< 4.8	3	> 174
Ac(hE)G(Dab)D-CHO	**36**	5.80 ± 0.21	2	< 4.8*	1	> 10
Ac(Idc)(hE)G((*S*)-Me-THIQ)D-CHO	**37**	7.37 ± 0.13	5	4.96 ± 0.04	5	257
Ac(hE)G((*S*)-Me-THIQ)D-CHO	**38**	6.65 ± 0.11	5	< 5	4	> 45
Ac(Idc)(hE)(BnT)(Dab)D-CHO	**39**	7.14 ± 0.12	6	< 4.8	5	> 219
Ac(Idc)(hE)(BnT)((*S*)-Me-THIQ)D-CHO	**40**	5.58 ± 0.08	3	< 4.8	4	> 6.0
Ac(Idc)(hE)V(Dab)D-CHO	**41**	6.55 ± 0.06	3	< 5	3	> 36
Ac(hE)V(Dab)D-CHO	**42**	< 5	2	< 4.8*	1	1.0
Ac(Idc)(hE)V((*S*)-Me-THIQ)D-CHO	**43**	6.75 ± 0.07	5	< 4.8	5	> 89
Ac(hE)V((*S*)-Me-THIQ)D-CHO	**44**	5.59 ± 0.08	4	< 4.8	3	> 6.2
Ac(Idc)(hE)(Tle)(Dab)D-CHO	**45**	6.22 ± 0.09	3	< 5	3	> 17
Ac(Idc)(hE)(Tle)((*S*)-Me-THIQ)D-CHO	**46**	5.68 ± 0.11	5	< 4.8	5	> 7.6
Linker series						
Idc(hE)GGD-CHO	**47**	7.92 ± 0.12	10	5.76 ± 0.13	8	145
Idc(hE)AVAD-CHO	**48**	< 4.8	3	< 4.8	3	1.0
Idc(hE)(Abz)D-CHO	**49**	< 4.8	2	< 4.8	3	1.0
Idc(hE)(Ambz)D-CHO	**50**	< 4.8	3	< 4.8	3	1.0
IdcGG(Dab)D-CHO	**51**	< 4.8	2	< 4.8	2	1.0

Downloaded from pubs.acs.org/jmcmar/article-pdf/doi/10.1021/acs.jmedchem.6c01370/6911434/jm6c01370.pdf by UNIV REGENSBURG user on 17 November 2026

https://doi.org/10.1021/acs.jmedchem.6c01370
J. Med. Chem. XXXX, XXX, XXX−XXX

Table 1. continued

		$pK_i \pm$ SEM				
sequence	cmpd	cpCasp2	*N*	Casp3	*N*	K_i (Casp3) / K_i (cpCasp2)
IdcGG((*S*)-Me-THIQ)D-CHO	**52**	< 4.8	3	< 4.8	4	1.0
Idc(AVA)(Dab)D-CHO	**53**	< 4.8	2	< 4.8	2	1.0
Idc(AVA)((*S*)-Me-THIQ)D-CHO	**54**	< 4.8	3	< 4.8	3	1.0
Ind(hE)(BnT)(Dab)D-CHO	**55**	5.94 ± 0.02	3	< 4.8	3	> 14

[a]Data shown are mean values ± SEM of *N* independent experiments, each performed in duplicate. Data were analyzed by nonlinear regression and were best fitted to sigmoidal concentration−inhibition curves. Calculated pK_i values derived from IC_{50} measurements. The reported pK_i values of **2**−**7** are cited from earlier publications. [b]Data ($pK_i \pm$ SD) described in Bresinsky et al.[25] [c]Data ($pK_i \pm$ SEM of N = 3) described in Singh et al.[26] [d]Data ($pK_i \pm$ SEM) described in Bresinsky et al.[28] [e]The error indicated corresponds to SD, not SEM. * Data should be considered preliminary (N = 1). Values reported as "<" indicate that 50 % inhibition was not achieved at the highest concentration tested in the corresponding assay.

Table 2. Enzyme Inhibitory Potency (pK_i Values) of Selected Pentapeptides 1−3, 6, 8, 10−12, 25, 32, 33, and 47 at Casp1, Casp4, Casp5, Casp6, Casp7, Casp8, Casp9, and Casp10[a]

sequence	cmpd	Casp1	*N*	SF Casp1	Casp4	*N*	SF Casp4	Casp5	*N*	SF Casp5	Casp6	*N*	SF Casp6	Casp7	*N*	SF Casp7	Casp8	*N*	SF Casp8	Casp9	*N*	SF Casp9	Casp10	*N*	SF Casp10
AcVDVAD-CHO	**1**	7.06 ± 0.06[a,c]	2	8.9		n.d.			n.d.		< 4[a,c]	2	> 10233	7.08 ± 0.06[a,c]	2	8.5		n.d.		5.57 ± 0.31[a,c]	2	275		n.d.	
AcVDV(Dab)D-CHO	**2**	5.43 ± 0.16[a,c]	2	68		n.d.			n.d.		< 4[a,c]	2	> 1820	4.61 ± 0.36[a,c]	2	447		n.d.		< 4[a,c]	2	> 1819		n.d.	
Idc(hE)V((*S*)-Me-THIQ)D-CHO	**3**	6.41 ± 0.12[b]	2	10		n.d.			n.d.		< 4[b]	2	> 2512	< 4[b]	2	> 2512		n.d.		5.12 ± 0.04[b]	2	191		n.d.	
AcVDV((*S*)-Me-THIQ)D-CHO	**6**	5.62 ± 0.05	3	186		n.d.			n.d.		< 4	3	> 7762	< 4	3	> 7762		n.d.		< 4	3	> 7762		n.d.	
AcVDV((*S*)-Br-THIQ)D-CHO	**8**	5.74*	1	158		n.d.			n.d.		< 4*	1	> 8710	4.85*	1	1230		n.d.		4.45*	1	3090		n.d.	
(Quin)VDV((*S*)-Me-THIQ)D-CHO	**10**	6.87 ± 0.08	2	5.9		n.d.			n.d.		4.18 ± 0.10	2	2884	5.16 ± 0.12	2	302		n.d.		4.77 ± 0.14	2	741		n.d.	
(Quin)VDV((*R*)-Me-THIQ)D-CHO	**11**	4.91*	1	5.4		n.d.			n.d.		4.55*	1	12	< 4*	1	> 44		n.d.		< 4*	1	> 44		n.d.	
(Quin)VDV((*S*)-Br-THIQ)D-CHO	**12**	6.78 ± 0.03	2	5.3		n.d.			n.d.		< 4	2	> 3162	5.25 ± 0.02	2	178		n.d.		4.87 ± 0.05	2	427		n.d.	
Idc(hE)(BnT)(Dab)D-CHO	**25**	5.81 ± 0.13	3	105	< 5	3	> 676	< 5	3	> 676	< 4	3	> 6761	< 4	3	> 6761	< 5	3	> 676	< 4	3	> 6761	< 5	3	> 676
Idc(hE)G(Dab)D-CHO	**32**	5.09 ± 0.15	3	472	< 5	3	> 525	< 5	3	> 525	< 4	3	> 5248	< 5	3	> 525	< 5	3	> 525	< 5	3	> 525	< 5	3	> 525
Idc(hE)G((*S*)-Me-THIQ)D-CHO	**33**	5.77 ± 0.04	3	151	6.08 ± 0.08	3	74	< 5	3	> 891	< 5	3	> 891	< 5	3	> 891	< 5	3	> 891	5.09 ± 0.10	3	724	< 5	3	> 891
Idc(hE)GGD-CHO	**47**	5.26 ± 0.06	3	457	< 5	3	> 832	< 5	3	> 832	< 5	3	> 832	< 5	3	> 832	< 5	3	> 832	4.55 ± 0.05	3	3244	< 5	3	> 832

[a]Data shown are mean values ±SEM of *N* independent experiments, each performed in duplicate. Data were analyzed by nonlinear regression and were best fitted to sigmoidal concentration−inhibition curves. Calculated pK_i values derived from IC_{50} measurements. The reported pK_i values of **1**−**3** are cited from earlier publications. SF (CaspX): selectivity factor toward cpCasp2 over CaspX, calculated from K_I(CaspX)/K_I(cpCasp2). [b]Data ($pK_i \pm$ SD) described in Bresinsky et al.[25] [c]Data ($pK_i \pm$ SEM of $N \geq 2$) described in Singh et al.[26] [d]The error indicated corresponds to SD, not SEM. [e]Data should be considered preliminary ($N = 1$). Values reported as "<" indicate that 50% inhibition was not achieved at the highest concentration tested in the corresponding assay. n.d. = not determined.

storage stability. CpCasp2 was first introduced by Cserjan-Puschmann and co-workers in 2020, who characterized the mutant cpCasp2 regarding substrate specificity and kinetic properties and compared it with the wild-type Casp2.[37] In the following, the term "selective" should be understood to refer to "selective over the tested caspase panel", since not all inhibitors were tested against all enzymes in the caspase family.

VDVAD Series

Inspired by the work of Maillard et al.,[20] who reported the racemic THIQ derivatives as P2 scaffolds, we incorporated the enantiopure (*S*)-6-Me-THIQ-COOH or (*S*)-6-Br-THIQ-COOH at the P2 position of the canonical inhibitor AcVDVAD-CHO (**1**) yielded AcVDV((*S*)-Me-THIQ)D-CHO (**6**) and AcVDV((*S*)-Br-THIQ)D-CHO (**8**), which showed a modest decrease in Casp2 inhibitory potency (pK_i = 7.89 and 7.94 vs. 8.01). However, this modification enhanced selectivity over Casp3, increasing it from 0.7-fold to 60- and 23-fold. Additional modification at P6 with the replacement of the acetyl group by quinaldic acid yielded the peptide (Quin)VDV((*S*)-Br-THIQ)D-CHO (**12**), which was accompanied by a further minor decrease in Casp2 inhibitory potency (pK_i = 7.50) and selectivity (5.5-fold over Casp3). Replacement of the (*S*)-bromo-substituted THIQ with (*S*)-6-Me-THIQ-COOH ((*S*)-Me-THIQ) had minimal impact on the potency and selectivity of the inhibitor. (Quin)VDV((*S*)-Me-THIQ)D-CHO (**10**) displayed a Casp2 pK_i of 7.64 and a Casp3/Casp2 selectivity of 14-fold. The peptides containing the *R*-configured THIQ analogs, AcVDV((*R*)-Me-THIQ)D-CHO (**7**), AcVDV((*R*)-Br-THIQ)D-CHO (**9**), (Quin)VDV((*R*)-Me-THIQ)D-CHO (**11**), and (Quin)VDV((*R*)-Br-THIQ)D-CHO (**13**), were largely inactive or showed negligible potency for both Casp2 and Casp3 (cf. Table 1). Substitution of the P3 and/or P5 valine with *α-tert*-leucine (Tle), to improve metabolic stability, yielded peptides **14**, **15**, and **16**, all of which retained high Casp2 inhibitory potency (pK_i = 7.90, 7.78, and 7.84, respectively). However, these modifications also increased Casp3 inhibitory potency (pK_i = 8.18, 8.17, and 8.26), diminishing the selectivity. Building on the previously published inhibitor AcVDV(Dab)D-CHO,[25] elongation of the P4 sidechain from aspartic acid to glutamic acid resulted in AcVEV(Dab)D-CHO (**19**), which showed a substantial reduction in Casp2 potency (pK_i = 5.14 vs. 7.26 for AcVDV(Dab)D-CHO[25]). Furthermore, replacing the terminal carboxylic acid of the P4 amino acid with an amide, as in AcVQV(Dab)D-CHO (**18**), completely abolished Casp2 activity. Neither peptide **18** nor **19** exhibited detectable activity on Casp3 (Table 1), suggesting that the presence of a free acidic group at P4 is critical for both Casp2 and Casp3 interactions. As reported previously, inhibitors containing serine at P2 are generally potent and exhibit a tendency toward Casp2

Downloaded from pubs.acs.org/jmcmar/article-pdf/doi/10.1021/acs.jmedchem.6c01370/6911434/jm6c01370.pdf by UNIV REGENSBURG user on 17 November 2026

https://doi.org/10.1021/acs.jmedchem.6c01370
J. Med. Chem. XXXX, XXX, XXX−XXX

selectivity.[28] Introduction of L-homoglutamic acid (hE) at the P4 position led to AcV(hE)GSD-CHO (**20**), which maintained good Casp2 potency (pK_i = 7.08) and increased the selectivity over Casp3 (23-fold). This confirms previous findings by Poreba et al. (2019) that L-homoglutamic acid at position P4 greatly enhances potency and selectivity.[21] Based on these favorable properties, L-homoglutamic acid was further investigated as a P4 substituent in the majority of the subsequently described peptides.

ITVKD Series

Based on the results from Bresinsky et al.,[28] further development was carried out in the ITVKD series. We applied the valine-to-*α-tert*-leucine exchange to the pentapeptide AcITVKD-CHO, generating compound **21** (AcIT(Tle)KD-CHO). This modification did not result in any significant change in Casp2 inhibitory potency (pK_i = 6.36 vs. 6.40 of AcITVKD-CHO[28]) and selectivity (1.7-fold over Casp3 vs. 2-fold[28]). Insertion of (*S*)-6-Me-THIQ-COOH at P2 led to compound **22** (AcITV((*S*)-Me-THIQ)D-COOH), but did not enhance Casp2 potency either (pK_i = 6.18 vs. 6.40 of AcITVKD-CHO[28]). However, a slight increase in selectivity over Casp3 was achieved (12-fold vs. 2-fold[28]), due to a decrease of Casp3 potency by about one log unit (Casp3 pK_i = 5.11 vs. 6.05 of AcITVKD-CHO[28]). Stepwise truncation of **22** yielded the tetrapeptide AcTV((*S*)-Me-THIQ)D-CHO (**23**) and the tripeptide AcV((*S*)-Me-THIQ)D-CHO (**24**), both of which displayed a complete loss of compound activity. This aligns with expectations, confirming the necessity of a five-amino acid motif for efficient Casp2 binding and interaction.[28]

Idc Series

In a previous study, Poreba et al.[21] demonstrated a significant increase in inhibitory potency and selectivity for Casp2 by introducing the sterically demanding, non-acetylated indoline-2(*S*)-carboxylic acid (Idc) at the P5 position. Building on these findings, together with Singh et al.,[26] and the above-mentioned favorable properties of hE at position P4, we synthesized a set of pentapeptide inhibitors with structural variations at the positions P2 and P3.

For inhibitor Idc(hE)(BnT)(Dab)D-CHO (**25**), *O*-benzyl-L-threonine (BnT) was used at P3 as a space-occupying structural feature to further elucidate structure−activity relationships within the S3 subsite of Casp2. Compound **25** showed high Casp2 inhibitory potency (pK_i = 7.62) and excellent selectivity over Casp3 (>6761-fold). The inhibitor Idc(hE)V(Dab)D-CHO (**27**) was synthesized to examine whether the exchange of (*S*)-Me-THIQ with diaminobutyric acid (Dab) at position P2 causes a loss of activity and selectivity in comparison to the previously published inhibitor Idc(hE)V((*S*)-Me-THIQ)D-CHO (**3**, MUR-65).[26] Fortunately, the activity (pK_i = 7.46 vs. 7.40) and selectivity (Casp3/Casp2 selectivity >457-fold vs. > 794-fold) for Casp2 were maintained at a comparable level. In an effort to improve enzymatic stability, *α-tert*-leucine was introduced at P3, resulting in Idc(hE)(Tle)(Dab)D-CHO (**28**). This substitution was associated with a minor decrease in Casp2 potency and a corresponding reduction in selectivity (Casp2 pK_i(Casp2) = 7.09; Casp3 pK_i (Casp3) < 4; and Casp3/Casp2 selectivity >195-fold).

Replacing Dab in compounds **25** and **28** with (*S*)-Me-THIQ led to Idc(hE)(BnT)((*S*)-Me-THIQ)D-CHO (**26**) and Idc(hE)(Tle)((*S*)-Me-THIQ)D-CHO (**29**), respectively. Both peptides exhibit substantially deteriorated pharmacological properties (Casp2 pK_i = 6.07 and <5; Casp3/Casp2 selectivity: 19 and n.d.). This indicates that the combination of bulky residues at both P2 and P3, such as (*S*)-THIQ and *α-tert*-leucine or *O*-benzyl-L-threonine, results in steric hindrance, leading to a marked loss in inhibitory potency. In contrast, space-occupying P3 residues paired with smaller P2 residues, such as Dab in **25** or **28**, or valine at P3 with (*S*)-THIQ, as in MUR-65, are well tolerated. These results collectively suggest that P3 can accommodate bulky substituents only when the adjacent P2 residue is sufficiently small or flexible, highlighting a structural constraint within the Casp2 S2−S3 binding region.

The most potent inhibitors in this series, with pronounced Casp2 selectivity, were pentapeptides in which the amino acid at position P2 or P3 was replaced by glycine. The compounds Idc(hE)G(Dab)D-CHO (**32**), Idc(hE)G((*S*)-Me-THIQ)D-CHO (**33**), and Idc(hE)VGD-CHO (**34**) all exhibited low nanomolar affinities (Casp2 pK_i = 7.72, 7.95, and 7.65) and Casp2 selectivity ranging from 302-fold to at least 832-fold (selectivity factors: >832, 537, and 302, respectively). However, **33** and **34** exhibited a slight increase in Casp3 activity (Casp3 pK_i = 5.22 and 5.17, respectively). In summary, these findings suggest that glycine at P2 or P3 is a favorable replacement. Previously, it was assumed that Dab or (*S*)-Me-THIQ at position P2 was essential for high inhibitory potency and selectivity toward Casp2. Inhibitor **34** has disproved this assumption, thus allowing higher structural variability in the design of future selective Casp2 inhibitors, especially regarding the optimization of physicochemical properties.

Introduction of a 5-fluoro-substituted (*S*)-Me-THIQ at P2 generated Idc(hE)V((*S*)-Me-THIQ*)D-CHO (**30**), which demonstrated moderate to high Casp2 potency (pK_i = 7.03) while exhibiting no detectable activity on Casp3. As expected, the *R*-configured equivalent (**31**) showed markedly reduced Casp2 potency (Casp2 pK_i = 5.44) and no inhibitory potency at Casp3 (Casp3 pK_i < 4.8).

Ac Series

Given the critical role of the P5 position in substrate binding, we investigated whether *N*-terminal acetylation of our inhibitors affects their inhibitory potency for Casp2.

N-Acetylation of potent compound **32** led to Ac(Idc)(hE)G(Dab)D-CHO (**35**) and was accompanied by a decrease of Casp2 inhibitory potency by about 0.5 log units. Similar effects were observed for the acetylated pentapeptides Ac(Idc)(hE)G((*S*)-Me-THIQ)D-CHO (**37**), Ac(Idc)(hE)(BnT)(Dab)D-CHO (**39**), Ac(Idc)(hE)(BnT)((*S*)-Me-THIQ)D-CHO (**40**), Ac(Idc)(hE)V(Dab)D-CHO (**41**), Ac(Idc)(hE)V((*S*)-Me-THIQ)D-CHO (**43**), and Ac(Idc)(hE)(Tle)(Dab)D-CHO (**45**), all showing decreases in Casp2 pK_i ranging from 0.4 to 0.9 log units. The only exception to this trend was Ac(Idc)(hE)(Tle)((*S*)-Me-THIQ)D-CHO (**46**), for which a poor Casp2 pK_i value of 5.68 was determined.

Regarding Casp3 inhibitory potency, we did not observe an impact of *N*-acetylation across this series of compounds. The reduction in Casp2 inhibition likely results from disrupted interactions between the free *N*-terminal amine and the Casp2 S5 subsite, supporting that the pentapeptide is stabilized in the Casp2 binding pocket through interactions with the *N*-terminal amine group.

Some pentapeptide inhibitors were truncated by removing the Idc moiety, resulting in acetylated tetrapeptides. These included Ac(hE)G(Dab)D-CHO (**36**), Ac(hE)G((*S*)-Me-THIQ)-CHO (**38**), Ac(hE)V(Dab)D-CHO (**42**), and Ac(hE)V((*S*)-Me-THIQ)D-CHO (**44**). Each of these compounds exhibited a

Downloaded from pubs.acs.org/jmcmar/article-pdf/doi/10.1021/acs.jmedchem.6c01370/6911434/jm6c01370.pdf by UNIV REGENSBURG user on 17 November 2026

https://doi.org/10.1021/acs.jmedchem.6c01370
J. Med. Chem. XXXX, XXX, XXX−XXX

further decrease in Casp2 potency of 0.9 to 1.4 log units compared to their pentapeptide counterparts. This, again, confirms that a complete pentapeptide scaffold is essential for high-potency Casp2 inhibition.[38]

Linker Series

In another attempt to decrease the molecular weight and the number of hydrogen bond donors and acceptors, multiple amino acids in the peptide backbone were exchanged, and the resulting compounds were tested for their inhibitory activity on Casp2 and Casp3. Initially, exchanging a single amino acid at the P2 or P3 position using glycine, as in compounds **32**, **33**, and **34**, led to high-potency Casp2 inhibitors. Subsequently, we investigated the insertion of linkers that span two amino acid positions, specifically P2−P3 and P3−P4.

Insertion of rigid spacers overcoming P2 and P3, such as 5-aminovalerianic acid (AVA), *para*-aminobenzoic acid (Abz), or *para*-aminomethylbenzoic acid (Ambz), resulted in a complete loss of activity. Compounds **48**, **49**, and **51** exhibited no detectable inhibitory potency for either Casp2 or Casp3 (Table 1). In contrast, incorporation of a more flexible glycine−glycine linker at the same position led to compound Idc(hE)GGD-CHO (**47**), which demonstrated high Casp2 activity (pK_i = 7.92), while the inhibitory potency for Casp3 was consistently low (pK_i = 5.76). These results suggest that the flexibility and peptidic nature of the glycine−glycine linker allow for a productive binding conformation, unlike the more rigid or non-peptidic AVA, Abz, and Ambz spacers.

Conversely, exchanging the positions P3 and P4 was not tolerated, regardless of the linker flexibility. Both rigid (5-aminovalerianic acid) and flexible (glycine−glycine) linkers at this site yielded inactive compounds. The peptides IdcGG(Dab)D-CHO (**51**), IdcGG((*S*)-Me-THIQ)D-CHO (**52**), Idc(AVA)(Dab)D-CHO (**53**), and Idc(AVA)((*S*)-Me-THIQ)D-CHO (**54**) demonstrated no detectable potency for Casp2 or Casp3 (pK_i < 4.8), suggesting that the spatial arrangement at the P3−P4 interface and the interaction of the acidic P4 side chain (D or hE) in the S4 subsite are critical for effective inhibitor binding and cannot accommodate such structural constraints.

For the most potent inhibitors, the nominal enzyme concentration approaches the calculated K_i/pK_i values. While enzyme concentration-dependence experiments demonstrated largely consistent potency estimates across a 20-fold range of cpCasp2 concentrations, minor tight-binding contributions cannot be completely excluded for the most active compounds and should be considered when interpreting absolute K_i/pK_i values. Exemplary data for compounds **1**, **25**, **32**, **33**, and **47** addressing this topic are shown in Figure S207 (Supporting Information). However, in jump-dilution experiments (Figure S210, Supporting Information), compounds **25**, **32**, **33**, and **47**—together with reference AcVDVAD-CHO—appear to bind Casp2 in a reversible manner as indicated by the short target residence time (<20 min), when comparing with irreversible reference compound emricasan (estimated >800 min).

Caspase Panel Assay

Beside reference compounds **1**−**3**, selected peptides (**6**, **8**, **10**, **11**, **12**, **25**, **32**, **33**, and **47**) were evaluated in a caspase panel assay to additionally determine their inhibitory potency for Casp1, 6, 7, and 9 (Table 2). Compounds **25**, **32**, **33**, and **47** were additionally evaluated at Casp4, Casp5, Casp8, and Casp10. None of the tested inhibitors showed significant inhibitory potency for Casp6, 7, or 9, indicating high specificity for Casp2. However, several compounds exhibited moderate inhibition of Casp1. In particular, the peptides bearing quinaldic acid at the P6 position, (Quin)VDV((*S*)-Me-THIQ)D-CHO (**10**) and (Quin)VDV((*S*)-Br-THIQ)D-CHO (**12**), displayed three-digit nanomolar affinities for Casp1 (pK_i = 6.87 ± 0.08 (mean ± SEM, N = 2) and 6.78 ± 0.03 (mean ± SEM, N = 2)). In contrast to the acetyl group, the larger aromatic quinaldic acid scaffold extends beyond the P5 region and may engage additional interactions that influence selectivity across the caspase family. This observation suggests that structural elements outside the canonical substrate recognition sequence can contribute to the overall selectivity profile. Among all tested compounds, inhibitors **25** (Idc(hE)(BnT)(Dab)D-CHO), **32** (Idc(hE)G(Dab)D-CHO), **33** (Idc(hE)G((*S*)-Me-THIQ)D-CHO), and **47** (Idc(hE)GGD-CHO) exhibited the most favorable selectivity profiles over the tested caspase panel, with at least 676-fold (**25**), 525-fold (**32**), 537-fold (**33**), and 145-fold (**47**) selectivity over caspases-3, -4, -5, -6, -7, -8, -9, and -10. It is interesting to note that compounds **25** (Casp1: 105-fold) and **33** (Casp1: 151-fold; Casp4: 74-fold) bearing sterically highly demanding residues in P2 or P3 exhibit somewhat lower selectivity over Casp1 or/and Casp4 (cf. Figure 3 and Table 2). Structurally, **25** is the only one of the four compounds containing benzylthreonine (BnT) that has a significantly more sterically bulky P3 group and Dab at P2, whereas **32**, **33**, and **47** all have glycine at P3. With regard to P2, compounds **32** (Dab), **33** ((*S*)-Me-THIQ), and **47** (G) are representatives of the three most favorable P2 amino acids in this series.

In Vitro Casp2-Catalyzed Tau Cleavage Assay

To assess the biochemical relevance of selected Casp2 inhibitors, we evaluated their effects on Casp2-catalyzed site-specific cleavage of tau, one of its physiological substrates. Inhibitors **3**, **32**, **33**, and **47** exhibited high Casp2 inhibitory potency and were tested in an in vitro Casp2 cleavage assay using purified recombinant proteins. All four inhibitors were equally effective in inhibiting the formation of Δtau314, the truncated, soluble tau fragment ending C-terminally at D314.[11] For the three compounds, comparable potencies were determined with IC_{50} values ranging from 1.77 μM to 2.65 μM (Figure 4). While these inhibitors displayed low-nanomolar affinities in fluorogenic peptide substrate assays, their apparent IC_{50} values in the tau cleavage assay were in the low-micromolar range. This apparent shift in potency is expected given the several differences between the two platforms. First, the tau cleavage assay requires significantly higher Casp2 concentrations to yield detectable levels of Δtau314, which raises the IC_{50} threshold for high-potency inhibitors. Second, full-length tau is a complex macromolecular substrate compared to fluorogenic peptides; thus, the steric hindrance and non-catalytic interactions between the enzyme and the large protein substrate as well as the extended assay duration may influence the binding equilibrium. Finally, semi-quantitative IP/Western blot detection of neo-epitopes may operate under distinct dynamic ranges compared to continuous kinetic fluorescence monitoring. It should be noted that while this in vitro cleavage assay confirms the inhibition of Casp2 activity using a full-length protein substrate, it does not demonstrate cellular target engagement, neuroprotection, or therapeutic efficacy. Future cellular and animal model studies will be necessary to evaluate target engagement and therapeutic potential in complex biological systems.

Downloaded from pubs.acs.org/jmcmar/article-pdf/doi/10.1021/acs.jmedchem.6c01370/6911434/jm6c01370.pdf by UNIV REGENSBURG user on 17 November 2026

https://doi.org/10.1021/acs.jmedchem.6c01370
J. Med. Chem. XXXX, XXX, XXX−XXX

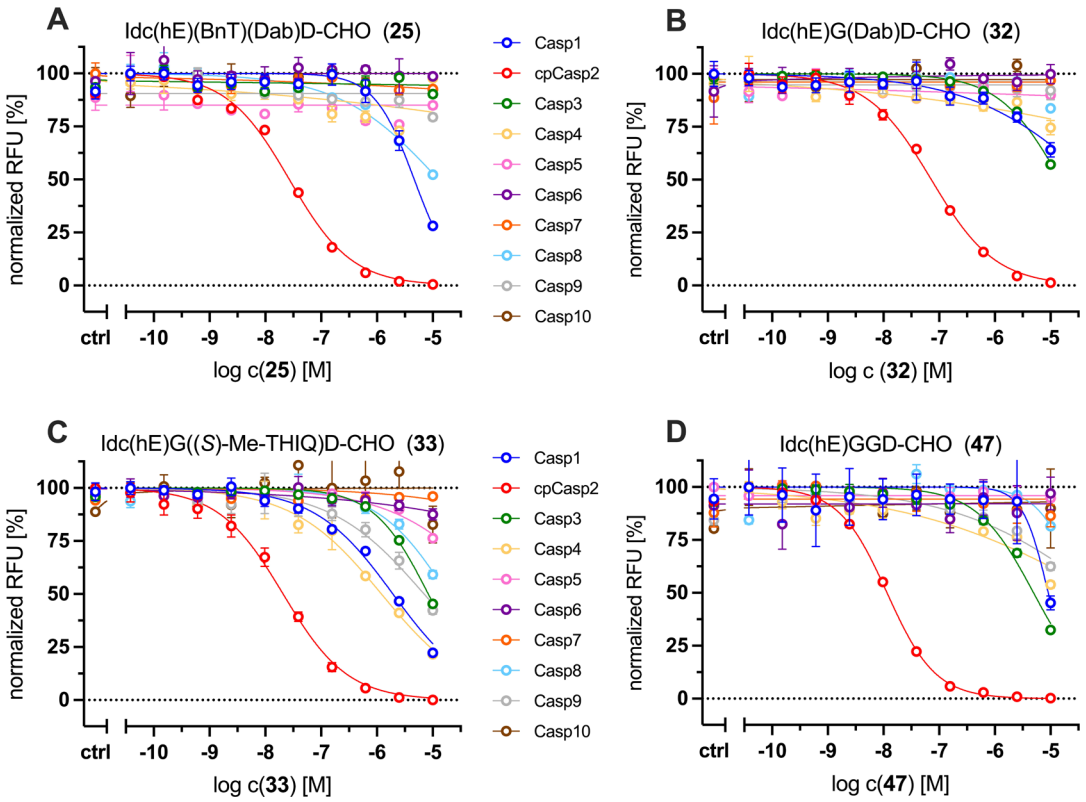


Figure 3. Representative curves from the caspase panel assay show the selectivity profile of potent Casp2 inhibitors **25** (A), **32** (B), **33** (C), and **47** (D) against Casp1, cpCasp2, Casp3, Casp4, Casp5, Casp6, Casp7, Casp8, Casp9, and Casp10. The relative fluorescent units (RFU) are normalized to the positive control (ctrl; corresponds to the measured RFU in the absence of an inhibitor) and represent the mean and standard deviation from a representative experiment, which was performed in duplicate. The pIC_{50} and ensuing pK_i values were calculated from three independent measurements using a four-parameter nonlinear regression fit with a variable slope and are reported in Table 2. Concentration−response curves with absolute RFU values for representative compounds (**25**, **32**, **33**, and **47**) against Casp1, cpCasp2, Casp3, Casp4, Casp5, Casp6, Casp7, Casp8, Casp9, and Casp10 together with the corresponding reference inhibitors for each enzyme are shown in the Supporting Information (Figure S209).

Physicochemical Properties

In order to assess the physicochemical properties of the compounds, we calculated the CNS MPO score (central nervous system multiparameter optimization), which combines fundamental physicochemical descriptors relevant to blood−brain barrier (BBB) permeability.[31] These are lipophilicity (ClogP), calculated partition coefficient at pH = 7.4 (ClogD), molecular weight (MW), topological polar surface area (TPSA), number of hydrogen-bond donors (HBD), and the most basic center (pK_a). Each parameter is weighted equally in the calculation and the score ranges from 0 to 6, whereby values ≥4 are considered favorable for passive BBB diffusion.[31] While none of the synthesized peptidic compounds reached the desired CNS MPO threshold (Table S1, Supporting Information), a slight improvement compared to earlier published peptidic inhibitors was obtained. The highest observed score, 3.7, was calculated for compound **24**, a tripeptide that did not exhibit any inhibitory activity against both Casp2 and Casp3. Among the most potent and selective inhibitors, compounds **25**, **32**, **33**, and **47**, CNS MPO scores ranged from 2.5 to 3.0, indicating no effective predicted CNS penetration, but an improvement compared to AcITVKD-CHO (**4**) or AcYDVKD-CHO (CNS MPO scores: 2.0).[25]

Oxidative Instability of Indoline-Containing Compounds

For compounds containing (*S*)-indoline-2-carboxylic acid at position P5, such as **25**, **27**, or **28**, a notable oxidative instability was observed. The indoline moiety is prone to aromatization into indole under both aqueous (1 mM) and nonaqueous (DMSO, 5 mM) conditions. However, decomposition in DMSO was less pronounced (Figure S1, Supporting Information). Quantification of the degradation product was not possible without an internal standard due to the formation of an aromatic system and a concomitant change of the extinction coefficient. Frozen aqueous stock solutions of these compounds demonstrated good stability over a 115-day period at −20 °C (Figures S2−S4, Supporting Information). The indole-containing degradation product of compound **25**, Ind(hE)(BnT)(Dab)D-CHO (**55**) (Figure 5), was isolated and investigated for Casp2 and Casp3 inhibition. Compared to the parent compound (pK_i = 7.83 and <4 for Casp2 and Casp3), the degradation product exhibited significantly reduced potency (pK_i = 5.94 and <4.8, respectively). Due to its sensitivity to oxidation, the Idc motif is not suitable for drug development. The described degradation was investigated for the aforementioned compounds but was also observed for MUR-90 and MUR-65 published by Singh et al. 2022[26] (compounds **1** and **3** in the respective publication). The observed degradation pathway is consistent with the well-documented oxidative aromatization of indoline derivatives to the corresponding indoles, a thermodynamically favorable transformation commonly reported in the medicinal and synthetic chemistry literature.[39,40] This inherent chemical liability provides a plausible explanation for the instability observed within the Idc-containing series. One

Downloaded from pubs.acs.org/jmcmar/article-pdf/doi/10.1021/acs.jmedchem.6c01370/6911434/jm6c01370.pdf by UNIV REGENSBURG user on 17 November 2026

https://doi.org/10.1021/acs.jmedchem.6c01370
J. Med. Chem. XXXX, XXX, XXX−XXX

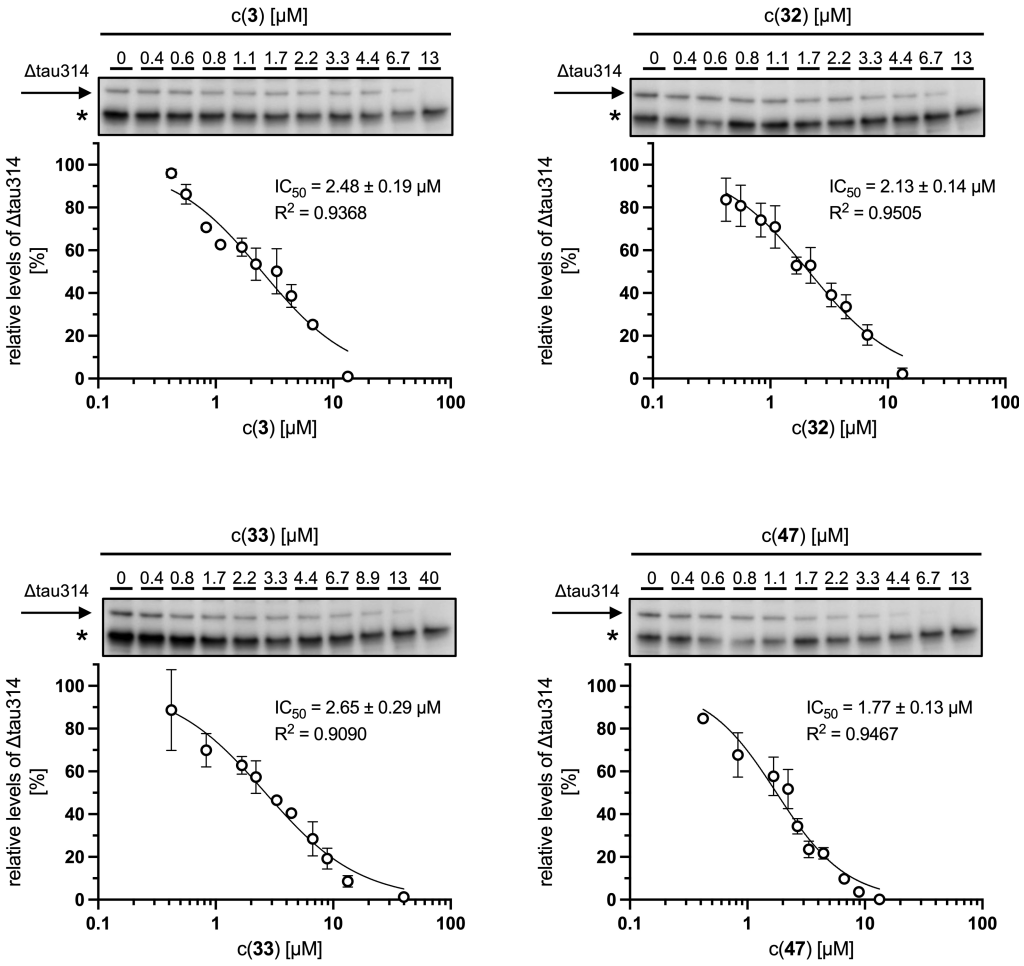


Figure 4. Casp2-selective inhibitors **3**, **32**, **33**, and **47** block enzyme-catalyzed Δtau314 formation in vitro. Representative immunoprecipitation (4F3)/Western blot (4F3-biotin) showing Δtau314 (arrow) and non-specific bands (*) in the presence of various concentrations of the respective compounds. The levels of Δtau314 (normalized to the no-compound control) and compound concentrations were fitted to a dose−response curve. The graphs show mean values (open circles) ± SD (error bars) of $N = 3$ independent experiments, each performed in duplicate.

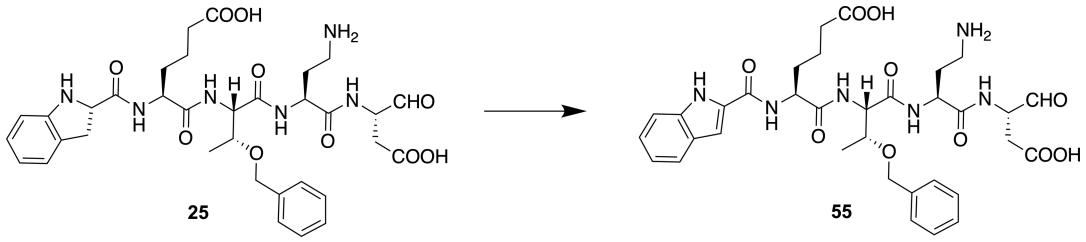


Figure 5. Chemical instability of Casp2 inhibitor **25**. In solution, the oxidation of indoline to indole occurs within a short period of time. The reaction is illustrated exemplarily for all indoline-containing Casp2 inhibitors.

strategy to mitigate this instability and the concomitant loss of activity of future compounds would be the introduction of a 2-methyl group into the indoline heterocycle.

ADME and Pharmacokinetic Profile of Compound 3 (MUR-65). *In Vitro ADME Data.* The previously published inhibitor Idc(hE)V((*S*)-Me-THIQ)D-CHO (**3**, MUR-65) served as an important starting point for scaffold optimization and is the aldehyde analog of the active nitrile-containing Casp2 inhibitor, MUR-90. As it is still ranked among the best compounds of the series, we assessed the physicochemical properties and the in vitro and in vivo pharmacokinetic performance of MUR-65. The calculated characteristics of the pentapeptide are summarized in Table S2 (Supporting Information). The CNS MPO score of 3.0, the number of six H-bond donors and 14 H-bond acceptors, the topological polar surface area (TPSA) of 211.3 Å^2, and the calculated logD of −0.8 reflect the polar character of the peptidomimetic. The data are confirmed by an experimental logD of −1.81 and a solubility of 277 μM for the TFA salt form in PBS (pH 7.4). The results from the MDCK-MDR1 permeability assay (Table S3, Supporting Information) show low membrane permeability both from apical and basolateral sides (apparent permeability coefficients $P_{app(A-B)} = 0.17 * 10^{-6}$ cm/s and $P_{app(B-A)} = 0.15*10^{-6}$ cm/s), suggesting limited ability of MUR-65 to penetrate the brain via passive

Downloaded from pubs.acs.org/jmcmar/article-pdf/doi/10.1021/acs.jmedchem.6c01370/6911434/jm6c01370.pdf by UNIV REGENSBURG user on 17 November 2026

https://doi.org/10.1021/acs.jmedchem.6c01370
J. Med. Chem. XXXX, XXX, XXX−XXX

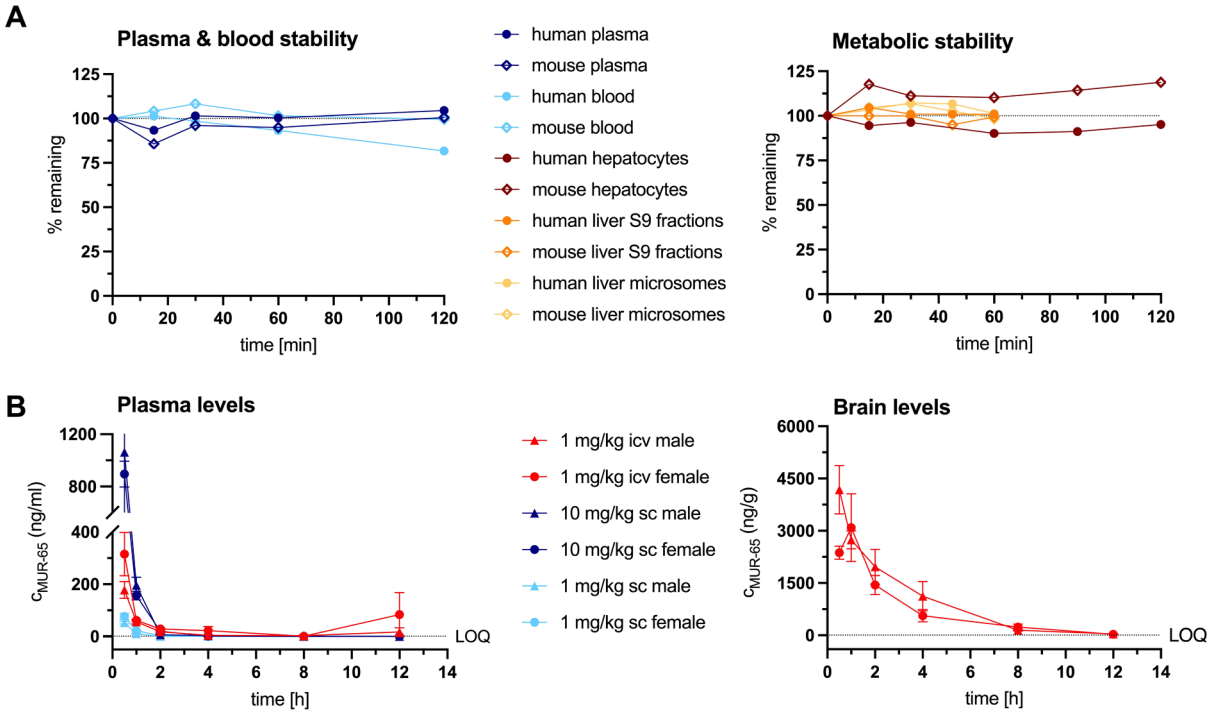


Figure 6. Pharmacokinetic profile of MUR-65 (**3**). In vitro ADME studies (**A**) show the stability of MUR-65 in human and mouse plasma and its metabolism in the liver depicted as the remaining percentage of the parent compound after different incubation times at 37 °C. A detailed visualization of the data including negative controls is provided in Figures S5 and S6 in the Supporting Information. In vivo PK studies (**B**) show the brain and plasma levels of MUR-65 after intracerebroventricular (icv) and subcutaneous (sc) injection in male and female CD1-mice. Graphs represent the mean ± SD of each study group, consisting of $N = 3$ animals for each administration route, dose, and sex. The dotted line marks the limit of quantification, which is 1 ng/mL for plasma and 5 ng/g for the brain.

diffusion. In addition, no MDR1-mediated efflux was observed (efflux ratio: 0.88). The low membrane permeability, high polarity and TPSA, and the high number of hydrogen-bond donors and acceptors collectively suggest poor BBB diffusion, representing a key challenge for the development of MUR-65 as a CNS-targeting inhibitor. Given the peptidic nature of the molecule, limited BBB penetration could already be anticipated from the chemical structure. In contrast, the general assumption that peptidomimetics are vulnerable to physiological degradation cannot be confirmed in the case of MUR-65: Despite the oxidative instability of indoline-containing compounds in PBS and DMSO (see the section above), MUR-65 remains almost unaffected in human and mouse plasma and blood samples except slight degradation in human blood (80% remaining parent drug after 2 h of incubation at 37 °C) (Figures 6A and S5A, Supporting Information) and showed moderate plasma protein binding (bound fraction of 44% (human) and 31% (mouse) (Figure S5B, Supporting Information). In addition, no metabolic degradation of MUR-65 was detected in human and mouse hepatocytes, liver S9 fractions or liver microsomes (Figures 6A and S6, Supporting Information), which also explains the lack of nonspecific reaction of the compound with SH donors such as glutathione or similar off-targets in plasma or liver. In summary, the potent and selective peptidomimetic Casp2 inhibitor MUR-65 shows the in vitro pharmacokinetic profile of a highly stable tool compound with insufficient membrane permeability as the remaining key challenge for administration.

In Vivo PK Data

To assess the pharmacokinetic profile of MUR-65 in vivo, the compound was administered via intracerebroventricular (icv) injection of 1 mg/kg and subcutaneous (sc) injection of 1 mg/kg and 10 mg/kg to male and female CD1 mice (cf. Figure 6B). The maximum levels (C_{max}) and corresponding timepoints (t_{max}), half-lives ($t_{1/2}$), dose-normalized area under the curves (AUC_{last}/D), and total brain plasma ratios K_p (Ratio AUC_{last}(brain)/AUC_{last}(plasma)) are summarized in the Supporting Information (Table S4). Although the icv application using cannulated mice is far from any clinical relevance, in vivo experiments using this administration route provide insights into the pharmacokinetic performance in brain tissue, which could be useful for future proof of mechanism studies regarding cpCasp2 inhibition in the context of neurodegenerative diseases. The brain half-life was calculated to be $t_{1/2\ brain} = 4.69$ h (male) and $t_{1/2\ brain} = 3.35$ h (female). The in vivo plasma half-lives ranged from 1.25 h (1 mg/kg, icv, female) to 1.96 h (10 mg/kg, sc, male), independently of the administration route and maximum plasma concentration. After icv injection, the brain/plasma ratio K_p (ratio AUC_{last}(brain)/AUC_{last}(plasma)) was found to be 51%/29% (1 mg/kg male/female). As indicated by low membrane permeability observed in in vitro data, the levels of MUR-65 that entered the brain after sc administration were all below the limit of quantification. Nevertheless, the injection resulted in maximum plasma levels of $C_{max} = 53.1$ ng/mL (male) and $C_{max} = 76.6$ ng/mL (female). The data shows the PK plasma profile of a pentapeptidic Casp2 inhibitor after subcutaneous administration and can be concluded with missing brain penetration as the main key challenge for future optimization.

Downloaded from pubs.acs.org/jmcmar/article-pdf/doi/10.1021/acs.jmedchem.6c01370/6911434/jm6c01370.pdf by UNIV REGENSBURG user on 17 November 2026

https://doi.org/10.1021/acs.jmedchem.6c01370
J. Med. Chem. XXXX, XXX, XXX–XXX

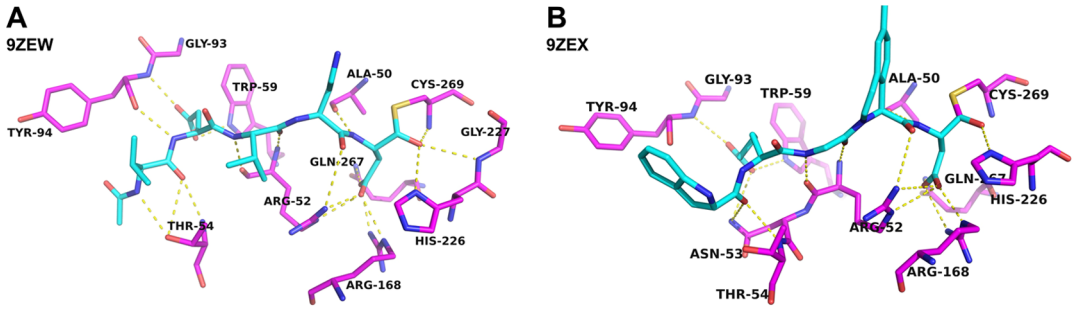


Figure 7. Comparison of experimentally determined JF1cpCasp2 complex inhibitor interactions. (**A**) The complex with covalently bound AcVDV(Dab)D-CHO (**2**) (PDB ID: 9ZEW). (**B**) Interactions for the complex with covalently bound Idc(hE)G((*S*)-Me-THIQ)D-CHO (**33**) (PDB ID 9ZEX). Both inhibitors display hydrogen bonding involving the P1 Asp (D_1) to Arg52, Arg168, and Gln267. In this and other Casp-2/3 structures, the sidechain carboxylate of the aspartic/homoglutamic acid in P4 makes H-bonds with the Trp59 sidechain nitrogen atom and Tyr94 main chain nitrogen atom.

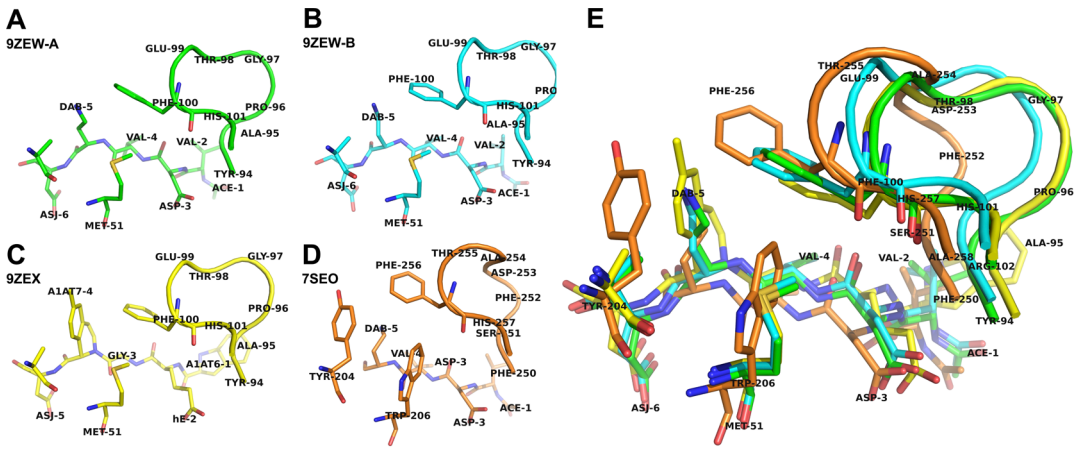


Figure 8. A comparison of Loop 4 conformation of experimentally determined JF1cpCasp2 complexes, with a representative canonical Casp2/Casp3 inhibitor (AcXDXXD-CHO). (**A**) The complex with covalently bound AcVDV(Dab)D-CHO (**2**) (PDB ID 9ZEW), monomer A. (**B**) The complex with covalently bound AcVDV(Dab)D-CHO (**2**) (PDB ID 9ZEW), monomer B. (**C**) The complex with covalently bound Idc(hE)G((*S*)-Me-THIQ)D-CHO (**33**) (PDB ID 9ZEX), (**D**) The complex with covalently bound AcVDV(DAB)D-CHO (PDB ID 7SEO). (**E**) Superpose of structures in (**A**), (**B**), (**C**), and (**D**) showing the plasticity of L4 in JF1cpCasp2 and bulky Tyr204 and Trp206.

Crystallography

Two peptide inhibitors, AcVDV(Dab)D-CHO (**2,** PDB ID 9ZEW) and Idc(hE)G((*S*)-Me-THIQ)D-CHO (**33,** PDB ID 9ZEX), were cocrystallized with JF1cpCasp2. The cocrystal structures were solved with high resolution (1.62 Å and 1.97 Å) and reported in further detail in Table S6, (Supporting Information). Information on non-standard residue definitions (Table S7), inhibitor composition and subsite assignment (Table S8), covalent linkage geometry (Table S9), mogul geometry validation of non-standard residues (Table S10), inhibitor atom naming (Table S11 and Figures S201 and S202), and residue definitions (Table S11) are provided in the SI. 9ZEW showed the higher quality of the two complexes (1.62 Å) and was therefore considered as the primary reference for SAR discussion (zero Ramachandran outliers (100th percentile), clashscore of 3, no bond-length or bond-angle outliers in either protein or inhibitor, and Real-Space Correlation Coefficient (RSCC) of 0.88−0.94). The complex 9ZEX (1.97 Å) shows excellent protein geometry (zero Ramachandran outliers, RMSZ 0.17−0.18). Data completeness is 48.8%, and the effective resolution, where completeness exceeds 50%, is approximately 2.5 Å. However, the non-standard residues A1AT6 ((2*S*)-indoline-2-carboxylic acid) and A1AT7 ((1*S*)-6-methyl-1,2-dihydro-isoquinoline-1-carboxylic acid) in this complex are flagged for geometry outliers (Table S10). These outliers are confined entirely to the ring systems, whereas no outliers occur at UN1 ((2*S*)-2-aminohexanedioic acid), ASJ ((3*S*)-3-amino-4-hydroxy-butanoic acid, "warhead"), at inter-residue peptide bonds, or the covalent Cys linkage. The five largest bond-length outliers (Z = 16.83−17.00) within A1AT6's indoline ring occur at the C23−C18 bond (observed 1.66−1.67 Å vs ideal 1.39 Å) and the C19−N bond (observed 1.67 Å vs ideal 1.39 Å). The outliers emerge from the comparison of the bound A1AT6 with the restraint dictionary, which was generated for the free, unlinked (2*S*)-indoline-2-carboxylic acid: In the free form, the ring nitrogen is a pyramidal sp^3 amine with short C−N bonds. However, in the covalent adduct, this nitrogen participates in a peptide bond to GL (the P2 linker), which delocalizes the nitrogen lone pair into the amide system, shifts the hybridization toward sp^2, and consequently lengthens the C19−N bond and reorganizes the ring junction angles. Therefore, the values in the deposited dictionary are inapplicable to the bonded form, and the outliers reflect correct bonded geometry, not a model error. A polder omit map for inhibitor **33** (9ZEX, Figure S200, Supporting Information) unambiguously supports the modeled atom positions and confirms that the ring geometry matches the experimental density. UN1 and ASJ, which are at the inter-residue junctions, have bond-length RMSZ of 0.83−0.95

Downloaded from pubs.acs.org/jmcmar/article-pdf/doi/10.1021/acs.jmedchem.6c01370/6911434/jm6c01370.pdf by UNIV REGENSBURG user on 17 November 2026

https://doi.org/10.1021/acs.jmedchem.6c01370
J. Med. Chem. XXXX, XXX, XXX−XXX

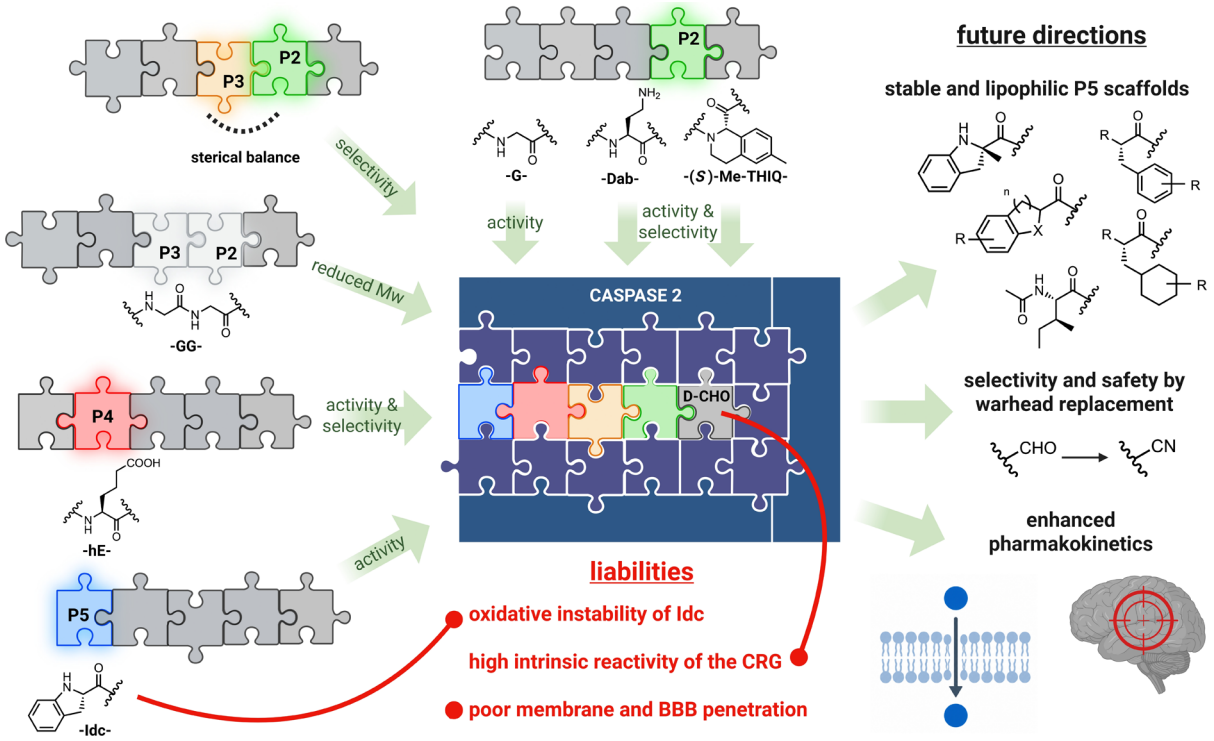


Figure 9. Summary of key SAR results, liabilities, and emerging starting points for further optimization of the pentapeptidic Casp2 inhibitors explored in this study. The figure was created with Biorender.com.

and zero bond-length outliers. This demonstrates that the refinement is well-behaved, and the issue is specific to the ring-containing residues, whose bonded geometry differs from the free-form dictionary.

The two crystal structures 9ZEW and 9ZEX have two and four copies of JF1cpCasp2 in the asymmetric unit, respectively. Each peptide inhibitor fits into the active site, adopts a substrate-like orientation, and forms a covalent link with the Cys269 of the catalytic dyad (Cys269-X-X-His266). The structures reveal extensive interactions between the peptide inhibitors and JF1cpCasp2 that span the catalytic S1−S5 sub-sites (Figure 7A,B). The P1 substituent (Asp-CHO), the highly conserved anchor point, occupies the S1 pocket, and its side-chain carboxylate forms salt bridges with the side chains of Arg52 and Arg168, as well as a hydrogen bond with the Nε atom of Gln267.

In the 9ZEW structure, the P4 side chain of the AcVDV(Dab) D-CHO inhibitor (Asp) is located in the S4 sub-site, forming direct hydrogen bonds between its carboxylate moiety and the indole nitrogen of Trp59 ($d_{O\text{-}N}$ = 3.1 and 3.0 Å in monomers A and B) and between its carboxylate moiety and the backbone nitrogen of Tyr94 ($d_{O\text{-}N}$ = 2.6 and 2.8 Å in monomers A and B). The S4 sub-site interactions are supplemented by a H-bond network bridged by water molecules. The water-mediated hydrogen bonds bridge the P4 group with the side chains of Asn53 and Arg91. In the 9ZEX structure, **33** has a homoglutamic acid (hE) at the S4 position, which has a longer side chain than the Asp at the corresponding S4 position of **2**. Despite the difference in side chain length, the P4 homoglutamic acid (hE) of **33** maintains a similar binding mode within the P4 pocket sub-site. The carboxylate ion forms a hydrogen bond with the Trp59 side chain ($d_{O\text{-}N}$ = 2.7, 3.1, 3.5, and 3.1 Å in monomers A, B, C, and D) and with the Tyr94 main chain nitrogen atom ($d_{O\text{-}N}$ = 2.8, 2.9, 3.0, and 3.1 Å in monomers A, B, C, and D).

The hydrophobic P2 (9ZEW), P3 (9ZEX), and P5 groups engage the S2, S3, and S5 pockets, establishing extensive van der Waals contacts. At S2 and S3 sites, the Phe100 side chain forms a supporting patch for the P2 side chain and P3 main chain. At the S5 site, Tyr94, Ala95, and Pro96 from loop4 (L4) form a hydrophobic patch, supporting P5 of the inhibitors. At the P3 position, 9ZEW has a relatively larger amino acid (Val), and **33** (9ZEX) has a small amino acid (Gly). The main chain of the inhibitor of **33** was pushed more than 1 Å toward L4. Phe100 also has a more than 1 Å movement to accommodate the bulky P3 amino acid, Val.

The structural comparison among 9ZEW, 9ZEX, and the Casp3 structure (PDB ID 7SEO[25]) shows that the 94−102 loop (JF1cpCasp2 numbering) plays an important role to the S4 pocket's architecture and its capacity to accommodate selective inhibitors (Figure 8). In the JF1cpCasp2 structures (9ZEW and 9ZEX), this loop exhibits significant conformational plasticity, which could influence the volume and accessibility of the S4 sub-site. In 9ZEW, the two monomers display distinct loop orientations that could be the reason for forcing the diaminobutyric acid (Dab) side chain into different conformations.

Due to the small Ala49 and a plasticity of the 94−102 loop, which create a spacious, adaptable pocket, bulky P2 groups like Dab or (*S*)-Me-THIQ in **33** have high inhibitory activity toward Casp2. However, the P2 pocket of Casp3 (7SEO) is limited by bulky Tyr204 and Trp206. Tyr204 acts as a rigid steric gatekeeper, physically precluding the binding of inhibitors with larger P2 substituents. Furthermore, we looked at various conformations in the sequence of the Casp2 L4 region (94−102). This identifies the Dab and (*S*)-Me-THIQ moieties as a key steric structural element and that the P2 position could play a key role in successful recognition, indicated by the specific conformation provided by the 94−102 L4 loop. Very similar

https://doi.org/10.1021/acs.jmedchem.6c01370
J. Med. Chem. XXXX, XXX, XXX−XXX

Downloaded from pubs.acs.org/jmcmar/article-pdf/doi/10.1021/acs.jmedchem.6c01370/6911434/jm6c01370.pdf by UNIV REGENSBURG user on 17 November 2026

interactions were observed at the P1 position. At the P4 position, **33** has a homoglutamic acid (hE)—the side chain position which is very similar to that of the 9ZEW inhibitor, with comparable interactions.

The crystal structures provide experimental support for several key binding interactions within the Casp2 active site and are consistent with the observed SAR trends. However, because crystal structures representing the complete range of P2/P3 substitution patterns investigated in this study are currently unavailable, mechanistic interpretations regarding the steric interplay between these positions should be regarded as SAR-supported hypotheses rather than definitive structural conclusions.

SUMMARY AND CONCLUSION

In this study, we developed a series of peptidic Casp2 inhibitors based on previously established SAR, aiming toward more potent and selective compounds with improved physicochemical properties. To explore a broader chemical space, we applied different strategies, including the introduction of more lipophilic moieties, linking single or multiple amino acid residues, and variation of amino acid side chains. Key findings of this SAR study, liabilities and future design approaches are summarized in Figure 9. Several novel pentapeptide inhibitors incorporating (*S*)-Me-THIQ, Dab, and especially glycine at P2 demonstrated high Casp2 inhibitory potency (with pK_i values up to 7.95) and excellent selectivity over Casp3. L-Homoglutamic acid at P4 proved indispensable for potency and especially Casp2 selectivity. Crystallographic studies provide insight into the underlying mechanism and show that hE in P4 is involved in a strong hydrogen-bonding network with the S4 binding site. Furthermore, bulky residues like Dab and (*S*)-Me-THIQ at P2 occupy a spacious pocket in cpCasp2, which is closed in Casp3 by bulky Tyr204 and Trp206, leading to Casp2 selectivity. Another structural constraint we observed was that bulky residues at both P2 and P3 caused a significant loss of activity, whereas small residues at P2 allowed for bulkier substituents at P3. This ligand-based SAR can be explained by the influence of the amino acid residues at positions P2 and P3 on the conformational arrangement of the inhibitor's backbone in the binding pocket. It was also confirmed that a pentapeptide backbone and a free *N*-terminal amine are critical for high-potency Casp2 inhibition. Truncation or *N*-acetylation of P5-Idc reduced potency, while the flexible glycine−glycine linker at P2−P3 was very well tolerated, in contrast to non-peptidic and rigid spacers. However, linking positions P3−P4 was not tolerated, regardless of the linker's flexibility or peptidic nature. Out of that series, compounds Idc(hE)G(Dab)D-CHO (**32**), Idc(hE)G((*S*)-Me-THIQ)D-CHO (**33**), and Idc(hE)GGD-CHO (**47**) emerge in terms of potency and selectivity over caspases-1, -3, -4, -5, -6, -7, -8, -9, and -10 and also effectively blocked Casp2-mediated tau cleavage in vitro, confirming their biochemical activities on a full-length protein substrate. While inhibition of pathological tau cleavage provides initial biological validation of Casp2 target modulation, additional studies examining intracellular target engagement, neuroprotective effects, and efficacy in disease-relevant models will be required to further assess the therapeutic potential of this inhibitor class. The different influences of the P2 amino acids on selectivity were interesting: (*S*)-Me-THIQ (P2 in **33**) showed limited selectivity for Casp1 and Casp4, whereas G (P2 in **47**) slightly increased the inhibitor potency at Casp3. The introduction of Dab at P2 (**32**) achieved the best selectivity balance in the caspase panel assay. While CNS permeability remains challenging (CNS MPO scores <4), compounds from this study have shown modest improvements. The indoline moiety, while beneficial for activity, was prone to oxidative degradation, making it unsuitable for drug development. Considering the results and limitations presented, compounds **32**, **33**, and **47** can be regarded as useful tool compounds for further studies. In future efforts, we will focus on enhancing the oxidative stability of indoline-containing scaffolds, for example, by introducing a 2-methyl group (Figure 9). Moreover, we plan to explore alternative P5 scaffolds that exhibit greater stability and are simultaneously advantageous regarding their physicochemical properties and Casp2 activity. The provided crystallographic analysis strengthens the contribution of lipophilic interactions between the P2, P3, and P5 amino acids and the JF1cpCasp2 binding pocket. In a previous publication, we reported a potent and selective Casp2 inhibitor containing a nitrile warhead (Idc(hE)V((*S*)-Me-THIQ)D-CN; pK_i = 8.12[26], which is challenging to prepare via solid-phase synthesis. Therefore, we want to identify and develop new nitrile-containing inhibitors that are more amenable to solid-phase synthesis while retaining high potency and selectivity. The respective aldehyde derivative Idc(hE)V((*S*)-Me-THIQ)D-CHO (**3**, MUR-65),[26] a potent and selective Casp2 inhibitor, has also been investigated in ADME and PK studies. MUR-65 demonstrates the in vitro pharmacokinetic profile of a highly stable lead compound with limited membrane and BBB penetration, posing a key challenge for successful application. Due to their high unspecific intrinsic reactivity against nucleophilic centers, e.g., cysteine or lysine side chains, aldehyde warheads are particularly prone to effective nonspecific reversible-covalent inhibition of off-target proteases, which is associated with safety liabilities. Consequently, the exploration of alternative warheads with reduced intrinsic reactivity may represent an important direction for further optimization. Future optimization efforts will focus on improving CNS exposure, metabolic stability, and overall drug-like properties through prodrug design, scaffold optimization, exploration of alternative warheads, and targeted delivery approaches. Such strategies may facilitate the development of next-generation Casp2 inhibitors with improved translational potential for neurodegenerative diseases.

EXPERIMENTAL SECTION

Chemistry

Commercially available chemicals, solvents, and the protected amino acids N-(9-fluorenylmethoxycarbonyl)-L-alanine (Fmoc-Ala-OH), 4-(9-fluorenylmethyloxycarbonyl)amino-benzoic acid (Fmoc-Abz-OH), 4-[9H-fluoren-9-ylmethoxycarbonyl(methyl)amino]benzoic acid (Fmoc-Ambz-OH), N-(9-fluorenylmethyloxycarbonyl)-5-amino-pentanoic acid (Fmoc-AVA-OH), N-(9-fluorenylmethoxycarbonyl)-L-aspartic-acid 4-*tert*-butyl ester (Fmoc-Asp(OtBu)-OH), N_α-Fmoc-N_γ-*tert*-butyloxycarbonyl-L-2,4-diaminobutyric acid (Fmoc-Dab(Boc)-OH), N_α-(9-fluorenylmethyloxycarbonyl)-L-glutamic-acid-gamma-t-butyl ester (Fmoc-Glu(OtBu)-OH), Fmoc-L-alpha-homoglutamic acid 6-*tert*-butyl ester (Fmoc-hE(OtBu)-OH), N-(9-fluorenylmethoxycarbonyl) glycine (Fmoc-Gly-OH), N-(9-fluorenylmethoxycarbonyl)-L-isoleucine (Fmoc-Ile-OH), (S)-N_α-(9-fluorenylmethyloxycarbonyl)-2-indolinecarboxylic acid (Fmoc-Idc-OH), N_α-(9-fluorenylmethoxycarbonyl)-N_ε-(*tert*-butoxycarbonyl)-L-lysine (Fmoc-Lys(Boc)-OH), N_α-(9-fluorenyl methoxycarbonyl)-L-glutamine (Fmoc-Gln-OH), quinaldic acid (Quin-OH), N-(9-fluorenylmethoxycarbonyl)-O-tert-butyl-L-serine (Fmoc-Ser(OtBu)-OH), Fmoc-F-Me-THIQ-OH, N-(9-fluorenyl

Downloaded from pubs.acs.org/jmcmar/article-pdf/doi/10.1021/acs.jmedchem.6c01370/6911434/jm6c01370.pdf by UNIV REGENSBURG user on 17 November 2026

https://doi.org/10.1021/acs.jmedchem.6c01370
J. Med. Chem. XXXX, XXX, XXX−XXX

methoxycarbonyl)-O-tert-butyl-L-threonine (Fmoc-Thr(OtBu)-OH), N-(9-fluorenylmethoxycarbonyl)-O-benzyl-L-threonine (Fmoc-Thr(Bn)-OH), N_{α}-(9-fluorenylmethyloxycarbonyl)-L-t-leucine (Fmoc-Tle-OH), and N-(9-fluorenylmethoxycarbonyl)-L-valine (Fmoc-Val-OH) were purchased from standard commercial suppliers (abcr (Karlsruhe, Germany), Acros Organics (Geel, Belgium), Alfa Aesar (Karlsruhe, Germany), BLD Pharmatech (Reinbek, Germany), Carbolution (St. Ingbert, Germany), Iris Biotech (Marktredwitz, Germany), Merck (Darmstadt, Germany), Sigma-Aldrich (Munich, Germany), and TCI Europe (Zwijndrecht, Belgium)) and were used as received. Deuterated solvents for nuclear magnetic resonance (^{1}H NMR and ^{13}C NMR) spectra were purchased from Deutero GmbH (Kastellaun, Germany). All reactions carried out with dry solvents were accomplished in dry flasks under a nitrogen or argon atmosphere. For the preparation of buffers, HPLC eluents, and stock solutions, Millipore water was used. Column chromatography was accomplished using Merck silica gel Geduran 60 (0.063−0.200 mm). Flash chromatography was performed using an Advion Interchim puriFlash XS 520 Plus purification system (Advion, Ithaca, NY; Interchim, Montluçon, France) with SI-HP 30 μm puriFlash columns from Interchim (Montlucon, France). The reactions were monitored by thin layer chromatography (TLC) on Merck silica gel 60 F254 aluminum sheets, and spots were visualized under UV light at 254 nm, by potassium permanganate or ninhydrin staining. Lyophilization was done with a Labogene CoolSafe 100-9 Pro equipped with a Welch CRV Pro 2 vacuum pump (Labogene, Allerød, Denmark). Nuclear magnetic resonance (^{1}H NMR and ^{13}C NMR) spectra were recorded on a Bruker (Karlsruhe, Germany) Avance 300 (^{1}H: 300 MHz, ^{13}C: 75 MHz), 400 (^{1}H: 400 MHz, ^{13}C: 101 MHz), 500 (^{1}H: 500 MHz, ^{13}C: 126 MHz), or 600 (^{1}H: 600 MHz, ^{13}C: 151 MHz) spectrometer using perdeuterated solvents. The chemical shift δ is given in parts per million (ppm). Multiplicities were specified with the following abbreviations: s (singlet), d (doublet), t (triplet), q (quartet), and m (multiplet), as well as combinations thereof. ^{13}C NMR peaks were determined by DEPT 135 and DEPT 90 (distortionless enhancement by polarization transfer). NMR spectra were processed with MestReNova 15.0 (Mestrelab Research, Compostela, Spain). High-resolution mass spectrometry (HRMS) was performed on an Agilent 6540 UHD Accurate-Mass Q-TOF LC/MS system (Agilent Technologies, Santa Clara, CA) using an ESI source. A preparative HPLC system from Thermo Fisher Scientific consisting of an UltiMate 3000 HPG-3200BX PUMP and a VWD-3400RS UV/Vis-detector is used for compound purification (Thermo Fisher Scientific, Waltham, MA). A Phenomenex Gemini 5 μm NX-C18 column (110 Å, 250 × 21.2 mm, Phenomenex Ltd., Aschaffenburg, Germany) served as the stationary phase. As the mobile phase, 0.1% TFA in Millipore water and acetonitrile (MeCN) were used. The temperature was 25 °C, the flow rate was 20 mL/min, and UV detection was performed at 220 nm. Analytical purity and stability control was performed on an 1100 HPLC system from Agilent Technologies equipped with an Instant Pilot controller, a G1312A binary pump, a G1329A ALS autosampler, a G1379A vacuum degasser, a G1316A column compartment, and a G1315B diode array detector (DAD) or on a Vanquish Core HPLC system from Thermo Fisher Scientific equipped with a Binary Pump C, a Split Sampler CT, Column Compartment C, a Diode Array Detector CG, and an ISQ EC Single Quadrupole Mass Spectrometer (Thermo Fisher Scientific, Waltham, MA). The column was a Phenomenex Kinetex XB-C18 column (250 × 4.6 mm 2.5 μm), Gemini 5 μm NX-C18 column (110 Å, 250 × 4.6 mm), or Gemini 3 μm NX-C18 column (110 Å, 150 × 3 mm) (Phenomenex Ltd., Aschaffenburg, Germany) tempered at 30 °C. As the mobile phase, mixtures of MeCN and aqueous TFA or mixtures of MeCN and aqueous formic acid were used (Method A: Kinetex XB-C18, linear gradient: MeCN/TFA (0.05%) (v/v) 0 min: 10:90, 25−35 min: 95:5, 36−45 min: 10:90 flow rate = 1.00 mL/min, t_0 = 2.75 min; Method B: Gemini 5 μm: linear gradient: MeCN/TFA (0.05%) (v/v) 0 min: 10:90, 25−35 min: 95:5, 36−45 min: 10:90; flow rate = 1.00 mL/min, t_0 = 2.90 min; Method C: Gemini 3 μm: 0.025% formic acid in MeCN/formic acid (0.05%) (v/v) 0 min: 10:90, 15−21 min: 95:5, 21.5−27 min: 10:90; flow rate = 0.50 mL/min, t_0 = 1.52 min). Capacity factors were calculated according to $k = (t_R - t_0)/t_0$. Detection was performed at 220 nm. Furthermore, filtration of the stock solutions with PTFE filters (25 or 15 mm, 0.2 μm, Phenomenex Ltd., Aschaffenburg, Germany) was carried out before testing. Compound purities determined by HPLC were calculated as the peak area of the analyzed compound in % relative to the total peak area (UV detection at 220 nm). All compounds were >95% pure by HPLC.

Synthesis and Analytical Data

General Procedures for Synthesis of the Peptides. The peptides were obtained by solid-phase peptide synthesis in 10 mL syringes by alternately coupling and deprotecting the respective N-terminal Fmoc-protected amino acids on an aspartic acid-loaded semicarbazide-amino Merrifield resin (150−600 mg) which was synthesized as previously reported.[28] The procedure is described below for an exemplary batch size of 300 mg resin (0.19 mmol, 1 equiv).

The aspartic acid-loaded semicarbazide amino-Merrifield resin (300 mg, 0.19 mmol, 1 equiv) was weighed into a fritted 10 mL syringe. Subsequently, 5 mL of a mixture of piperidine 20% in DMF was drawn to remove the N-terminal Fmoc-protecting group. The syringe was shaken on an orbital shaker at 35 °C for 15 min. The orbital shaker was covered with a box, which was insulated from the inside with aluminum foil. An infrared lamp was placed on an aperture on top. To keep the temperature constant at 35 °C, the lamp was controlled by a thermostat. The liquid was then removed with the aid of a vacuum flask, and the residual resin was washed with DMF (3 x 8 mL). The coupling of the amino acids to the N-terminus was performed by weighing the corresponding amino acid and HATU in two separate Erlenmeyer flasks. Subsequently, both were dissolved in 3−4 mL of a mixture of DMF/NMP (8/2 v/v), and DIPEA was added to the solution of HATU. As a rule, 5 equiv of the amino acid was used in combination with 5 equiv of HATU (357 mg, 0.94 mmol) and with 5 equiv of DIPEA (164 μL, 0.94 mmol). If the equivalents of the amino acid deviated from 5 equiv, the amounts of HATU and DIPEA were adjusted proportionally so that mmol always resulted in a ratio of 1:1. Subsequently, both solutions were drawn into the resin-loaded syringe and shaken at 35 °C for 45 min. The liquid was then removed with the aid of a vacuum flask, and the residual resin was washed with DMF (3 x 8 mL).

The coupling and deprotection steps were repeated until the desired tri-, tetra-, or pentapeptide was built up. Then, the N-terminal Fmoc protecting group was removed using piperidine in DMF (20%). Subsequently, the N-terminus of the peptide was acetylated by dissolving acetic anhydride (178 μL, 1.88 mmol, 10 equiv) and DIPEA (328 μL, 1.88 mmol, 10 equiv) in 6−8 mL of DMF. The solution was drawn into a syringe and shaken for 30 min at room temperature. After completion, the liquid was removed, and the resin was washed with DMF (2 x 8 mL), methanol (2 x 8 mL), dichloromethane (2 x 8 mL), and finally with diethyl ether (2 x 8 mL). The peptide was cleaved off the resin, and the side chains were deprotected by drawing up 6 mL of trifluoroacetic acid (TFA) at 90% in water. The syringe was shaken for 1 h at room temperature. The liquid was then poured into a round-bottomed flask. The step was repeated, the combined cleavage cocktail was diluted with 50 mL of water, and freeze-dried. The crude product was purified by HPLC, yielding the corresponding peptide.

For the synthesized peptides, the formation of an intramolecular hemiacetal between the carboxylic acid in the side chain of aspartic acid and the aldehyde at the C-terminus of the peptide was observed both in NMR spectroscopy (signal splitting) and HPLC chromatography (broadening of peaks). There are two possible diastereomers for the cyclic form, caused by the formation of an additional chiral center at the former aldehyde carbon. The equilibrium between the open-stranded form and the cyclic hemiacetal was considered for interpretation of the NMR spectra, whereby the signal splittings of aspartic acid, as these are the most pronounced, are described as follows: In ^{1}H spectra, the open-stranded form shows the signal of the aldehyde function (C**H**O) at 9.3 ppm (DMSO-d_6). The proton of the carboxylic acid is expected at ~12 ppm (DMSO-d_6) but can be distinguished from the COO**H** of homoglutamic acid only in very few instances. The hemiacetal form shows up in the C**H** signals at ~5.5 ppm (DMSO-d_6) and the corresponding O**H** at ~5.7 ppm (DMSO-d_6). The integration ratio of 2−3/8−7

Downloaded from pubs.acs.org/jmcmar/article-pdf/doi/10.1021/acs.jmedchem.6c01370/6911434/jm6c01370.pdf by UNIV REGENSBURG user on 17 November 2026

https://doi.org/10.1021/acs.jmedchem.6c01370
J. Med. Chem. XXXX, XXX, XXX−XXX

between the signal at 9.3 ppm (aldehyde) and 5.5 ppm (hemiacetal) shows that the cyclic form is favored in most of the peptides. Peaks and integrals of the neighboring C$\mathbf{H}_2$ in the aspartic acid side chain are split in the range of ∼2.2−3.2 ppm and were only labeled for the prominent hemiacetal isomer. In ^{13}C spectra, peaks at ∼200−210 ppm (**C**HO), at ∼103 ppm (**C**−OH), and at ∼90 ppm (**C**−OH) are aligned with the neighboring C$\mathbf{H}_2$ at ∼55 ppm, ∼53 ppm, and ∼48 ppm, respectively. For reasons of clarity, only the signal pair for the most pronounced diastereomer of the hemiacetal form was picked for the peak report. The quaternary carbon atom of the aldehyde (**C**HO) was additionally marked if it was particularly visible. A splitting of the signals in the ^{1}H and ^{13}C spectra can also be observed for other C and H atoms, but superposition makes precise separation and alignment difficult.

(3*S*,9*S*,12*S*)-9-(2-Aminoethyl)-3-(3-carboxypropyl)-12-formyl-1-((*S*)-indolin-2-yl)-1,4,7,10-tetraoxo-2,5,8,11-tetraazatetradecan-14-oic Acid Dihydrotrifluoroacetate (32). The title compound was synthesized according to the general procedure using 300 mg of resin (0.19 mmol, 1 equiv), Fmoc-Dab-OH (413 mg, 0.94 mmol, 5 equiv), Fmoc-Gly-OH (279 mg, 0.94 mmol, 5 equiv), Fmoc-hE(OtBu)-OH (165 mg, 0.38 mmol, 2 equiv), and Fmoc-Idc-OH (362 mg, 0.94 mmol, 5 equiv), yielding a fluffy white solid (16 mg, 11%): RP-HPLC: >99% (Method B: $t_R = 6.67$, $k = 1.30$). ^{1}H NMR (500 MHz, DMSO-d_6) δ 12.12 (brs, 1H), 9.43 (d, J = 2.4 Hz, 0.1H), 8.57−7.91 (m, 4H), 7.82−7.69 (m, 3H), 7.15−6.76 (m, 3H), 6.63−6.58 (m, 1H), 6.05 (t, J = 4.8 Hz, 0.3H), 5.76 (t, J = 5.0 Hz, 0.2H), 5.55−5.41 (m, 0.4H), 4.52−4.36 (m, 1H), 4.34−4.24 (m, 2H), 4.15−4.06 (m, 1H), 3.76−3.73 (m, 1H), 3.35−3.27 (m, 1H), 3.06−2.87 (m, 2H), 2.87−2.69 (m, 3H), 2.42−2.25 (m, 1H), 2.23−2.16 (m, 2H), 2.00−1.89 (m, 1H), 1.89−1.76 (m, 1H), 1.74−1.66 (m, 1H), 1.59−1.42 (m, 3H). ^{13}C NMR (126 MHz, DMSO-d_6): δ 174.83, 173.74, 172.25, 171.13, 170.24, 158.43, 151.38, 127.85, 127.69, 124.68, 118.66, 109.81, 102.94, 61.20, 53.00, 52.36, 50.65, 43.36, 42.51, 36.54, 34.93, 33.70, 33.46, 32.15, 21.19. HRMS (ESI-MS): m/z [M + H$^+$] calcd for $C_{25}H_{35}N_6O_9^+$: 563.2460, found 563.2464; $C_{25}H_{34}N_6O_9$ x 2 $C_2HF_3O_2$ (790.63).

(*S*)-6-((2-((*S*)-1-(((*S*)-1-Carboxy-3-oxopropan-2-yl)carbamoyl)-6-methyl-3,4-dihydroisoquinolin-2(1*H*)-yl)-2-oxoethyl)amino)-5-((*S*)-indoline-2-carboxamido)-6-oxohexanoic Acid Hydrotrifluoroacetate (33). The title compound was synthesized according to the general procedure using 500 mg of resin (0.31 mmol, 1 equiv), Fmoc-(*S*)-Me-THIQ-OH (BB2) (269 mg, 0.63 mmol, 2 equiv), Fmoc-Gly-OH (465 mg, 1.56 mmol, 5 equiv), Fmoc-hE(OtBu)-OH (344 mg, 0.78 mmol, 2.5 equiv), and Fmoc-Idc-OH (603 mg, 1.56 mmol, 5 equiv), yielding a fluffy white solid (78 mg, 33%): RP-HPLC: 97% (Method C: $t_R = 8.35$, $k = 4.49$). ^{1}H NMR (500 MHz, DMSO-d_6): δ 11.59 (brs, 1H), 9.47−9.24 (m, 0.1H, CHO), 9.09−7.93 (m, 3H), 7.42−7.22 (m, 1H), 7.17−6.93 (m, 4H), 6.86−6.61 (m, 2H), 5.75−5.61 (m, 0.6H), 5.55−5.44 (m, 1H), 5.44−5.23 (m, 0.8H), 4.71−4.55 (m, 1H), 4.47−4.39 (m, 1H), 4.36−4.29 (m, 1H), 4.27−3.76 (m, 4H), 3.61−3.24 (m, 2H), 3.02−2.75 (m, 3H), 2.37−1.96 (m, 6H), 1.78−1.62 (m, 1H), 1.61−1.36 (m, 3H). ^{13}C NMR (126 MHz, DMSO-d_6): δ 174.73, 172.82, 171.95, 171.41, 168.67, 158.87, 158.57, 137.10, 135.60, 129.46, 129.09, 128.96, 128.58, 127.79, 127.47, 124.87, 119.96, 110.96, 102.86, 72.15, 60.99, 57.87, 52.91, 52.21, 41.56, 41.47, 35.00, 33.76, 33.72, 32.56, 28.54, 21.21, 21.11. HRMS (ESI-MS): m/z [M + H$^+$] calcd for $C_{34}H_{38}N_5O_9^+$: 636.2664, found 636.2666; $C_{34}H_{37}N_5O_9$ x $C_2HF_3O_2$ (749.70).

(3*S*,12*S*)-3-(3-Carboxypropyl)-12-formyl-1-((*S*)-indolin-2-yl)-1,4,7,10-tetraoxo-2,5,8,11-tetraazatetradecan-14-oic Acid Dihydrotrifluoroacetate (47).

The title compound was synthesized according to the general procedure using 600 mg of resin (0.38 mmol, 1 equiv), Fmoc-Gly-OH (558 mg, 1.88 mmol, 5 equiv), Fmoc-Gly-OH (558 mg, 1.88 mmol, 5 equiv), Fmoc-hE(OtBu)-OH (330 mg, 0.76 mmol, 2 equiv), and Fmoc-Idc-OH (289 mg, 0.76 mmol, 2 equiv), yielding a fluffy white solid (42 mg, 18%): RP-HPLC: 95%, (Method B: $t_R = 8.17$, $k = 1.82$). ^{1}H NMR (600 MHz, DMSO-d_6): δ 12.03 (brs, 1H), 9.42 (s, 0.1H), 8.49−7.74 (m, 4H), 7.22−6.79 (m, 3H), 6.76−6.57 (m, 1H), 6.17−6.00 (m, 0.3H), 5.98−5.64 (m, 1H), 5.49 (d, J = 5.4 Hz, 0.1H), 4.98−4.03 (m, 3H), 3.94−3.61 (m, 4H), 3.59−3.35 (m, 1H), 3.08−2.83 (m, 2H), 2.80−2.53 (m, 1H), 2.22−2.14 (m, 2H), 1.75−1.40 (m, 4H). ^{13}C NMR (151 MHz, DMSO-d_6): δ 200.34 (CHO), 175.43, 174.71, 173.78, 172.91, 172.39, 169.53, 151.54, 127.65, 124.65, 121.60, 118.51, 109.70, 102.95, 61.23, 59.40, 52.91, 49.40, 42.56, 34.92, 33.68, 33.51, 32.16, 21.17. HRMS (ESI-MS): m/z [M + H$^+$] calculated for $C_{23}H_{30}N_5O_9^+$: 520.2038, found 520.2045; $C_{23}H_{29}N_5O_9$ x $C_2HF_3O_2$ (633.53).

Fluorescent Enzyme Assay Protocols

Biochemical Reagents. Human recombinant Casp1, 4, 5, 6, 7, 8, 9, and 10 were purchased from Enzo Life Sciences (Lörrach, Germany). AFC fluorogenic substrates (AcYVAD-AFC, Z-VDVAD-AFC, AcDEVD-AFC, ACWEHD-AFC, Z-VEID-AFC, AcIETD-AFC, and AcLEHD-AFC) and control peptides (AcYVAD-CHO, AcVDVAD-CHO, AcDEVD-CHO, AcWEHD-CHO, AcVEID-CHO, AcIETD-CHO, and AcLEHD-CHO) were purchased from Bachem (Babendorf, Switzerland) and MedChemExpress (Monmouth Junction, New Jersey, US). Recombinant Casp2, cpCasp2, Casp3, and tau were produced in-house as described in the following. Enzymes were not active-site-titrated.

Expression and Purification of Recombinant Casp2 and Tau. The genes encoding the human Casp2 p19 and p12 subunits were cloned into the pCOLADuet-1 vector (MilliporeSigma) as two separate open reading frames. The DNA sequence for the human microtubule-associated protein Tau (0N4R isoform) was cloned into the pET28a expression vector (MilliporeSigma) between the *NdeI* and *XhoI* restriction sites. The resulting construct encodes a 403-amino-acid protein consisting of an N-terminal 20-amino-acid His-tag fusion, followed by the 383-amino-acid human 0N4R tau sequence. The construct was verified by Sanger DNA sequencing. Both vectors were transformed into the BL21(DE3) *E. coli* strain (MilliporeSigma). Protein expression was induced by adding 150 μM isopropyl-β-*D*-thiogalactopyranoside (IPTG) (Promega), followed by incubation at room temperature for 16 h with shaking at 250 rpm.

For purification, cells were harvested by centrifugation at 4,000*g* for 15 min at 4 °C, resuspended in lysis buffer (100 mM Tris-HCl, 100 mM NaCl, pH 8.0), and sonicated on ice. Soluble lysates were isolated via high-speed centrifugation (48,300*g* for 30 min at 4 °C). The supernatant, containing the soluble recombinant protein, was purified using HisPur Ni-NTA resin (Thermo Fisher Scientific). The resin was washed with wash buffer (100 mM Tris-HCl, 100 mM NaCl, 40 mM imidazole, pH 8.0), and bound proteins were eluted using elution buffer (100 mM Tris-HCl, 100 mM NaCl, 500 mM imidazole, pH 8.0). Finally, purified proteins were subjected to buffer exchange using Amicon filter Units (MWCO = 10 kDa) to 1x phosphate-buffered saline (pH 7.4) and stored at −80 °C.

Expression and Purification of Recombinant Circularly Permutated Caspase-2 (cpCasp2). A circularly permutated caspase-2 (cpCasp2) based on modifications to Casp2 (UniProt P42575) suggested by Cserjan-Puschmann et al.[37] was expressed. The gene encoding 6H-Casp2$_{334-452}$-GS-Casp2$_{170-333}$ with a D$_{347}$ → A$_{347}$ mutation was inserted into a pET30a(+) vector (GenScript, Piscataway, NJ, USA) using NdeI and EcoRV restriction sites. The transformation into Lemo21 cells was performed as recommended by the vendor (New England Biolabs, Ipswich, MA, USA), and the plates were incubated overnight at 37 °C. A single colony was picked for primary culture using a sterile tip, added to sterile Luria broth (LB) media containing antibiotics, and incubated overnight at 37 °C and 270 rpm. The primary culture was then diluted 1:100 into 1 L shake flasks containing sterile LB and the proper antibiotics. The liter cultures were incubated at 37 °C and 270 rpm, and the OD was monitored until it reached between 0.6 and 0.8. Once the desired OD was reached, the cells were induced overnight with 0.1 mM IPTG at 28 °C and 270 rpm. After induction, the cells were harvested through centrifugation at 5000*g* for 20 min. The typical yield was about a 3.5 g of cell pellet per liter. The pellets were stored at −20 °C until purification. The pellets were resuspended in lysis buffer (buffer A with 2.5 μM Leupeptin, 5 μM

Downloaded from pubs.acs.org/jmcmar/article-pdf/doi/10.1021/acs.jmedchem.6c01370/6911434/jm6c01370.pdf by UNIV REGENSBURG user on 17 November 2026

https://doi.org/10.1021/acs.jmedchem.6c01370
J. Med. Chem. XXXX, XXX, XXX−XXX

Pepstatin, 0.5 μM DNase, 1 mM PMSF, and 10 mM $MgCl_2$) and lysed through sonification. The lysate was clarified through centrifugation at 20,000*g* for 30 min. The supernatant was filtered through a 0.45 μm filter before it was purified on a BioRad Biologic DuoFlow Chromatography System. For nickel-affinity chromatography, a 5 mL HisTrap FF column was equilibrated with 100% buffer A (100 mM Tris, pH 8.0, 100 mM NaCl, 20 mM imidazole). A gradient of buffer B (100 mM Tris, pH 8.0, 100 mM NaCl, and 400 mM imidazole) was then applied from 0 to 50% to wash and elute the protein. cpCasp2 was eluted at about 20% buffer B. Final purification was achieved on a Hi-Trap Q anion exchange column in 25 mM Tris, pH 8.0, utilizing a gradient of 0−1 M NaCl. cpCasp2 was eluted at about 150 mM NaCl. The final yield was 8−10 mg of cpCasp2 per liter. After adding 10% glycerol, the protein was stored at −80 °C.

Expression and Purification of Recombinant Casp3. The pET23b vector encoding human Casp3 was a gift of Dr. Michelle Arkin from the University of California, San Francisco. Expression and purification of Casp3 was guided by previously described protocols.[41] Briefly, the plasmid was transformed into *E. coli* Rosetta 2 pLyss DE3 cells that were cultured at 1 L scale in shake flasks at 37 °C. Five hours post induction with IPTG, the cells were harvested through centrifugation (5000*g* for 15 min at 4 °C), lysed by sonication, and centrifuged again for 30 min at 20,000*g*. The supernatant was resuspended in buffer (100 mM Tris pH 8.0, 500 mM NaCl). Purification was performed on a Cytiva ÄKTA Pure system (Marlborough, MA) by nickel-affinity chromatography on a HisTrap FF crude column (Cytiva), followed by ion-exchange chromatography on a HiTrap Q FF column (Cytiva). Protein was diluted to 0.5 mg/mL and stored at −80 °C in 100 mM Tris, pH 8.0, supplemented with 10% glycerol. The typical yield for the expression, isolation, and purification was approximately 3 mg/L.

Fluorometric Enzyme Assay

K_M values were determined experimentally for every enzyme batch to be the following: Casp1: 11.5 μM; cpCasp2: 13.6 μM and 19.0 μM; Casp3: 17.2 μM and 5.6 μM; Casp4: 46.6 μM; Casp5: 110.4 μM; Casp6: 53.5 μM; Casp7: 26.5 μM; Casp8: 29.8 μM; Casp9: 79.2 μM; and Casp10: 344.5 μM. Enzymes were diluted in aqueous buffer consisting of 100 mM MES (pH 6.5) for Casp2 and 100 mM HEPES (pH 7.0) for all other caspases, plus 150 mM NaCl, 0.1% CHAPS, and 1.5% sucrose. Dithiothreitol (DTT) was added from frozen stock solution (stored at −20 °C) freshly to buffer immediately prior to performing the assay, resulting in a final assay concentration of 10 mM. Enzyme concentrations were 0.1 U/well for Casp1, Casp6, and Casp7, 20 nM/well for Casp2, 2 nM/well for Casp3, and 0.05 U/well for Casp4, Casp5, Casp8, Casp9, and Casp10. 14 μL/well of enzyme solution was placed in a black 384-well Corning assay plate. Starting from DMSO stock solutions, test compounds were serially diluted in assay buffer without DTT, and 2 μL/well was plated into the assay plate in duplicate. The final DMSO assay concentration was kept below 0.16%. The compound and enzyme mixture was incubated at 37 °C for 5 min before 4 μL of the AFC substrate (final assay concentrations: 5 μM AcYVAD-AFC for Casp1, 10 μM Z-VDVAD-AFC for Casp2, 5 μM AcDEVD-AFC for Casp3, 10 μM AcWEHD-AFC for Casp4, 25 μM AcWEHD-AFC for Casp5, 5 μM Z-VEID-AFC for Casp6, 5 μM AcDEVD-AFC for Casp7, 10 μM AcIETD-AFC for Casp8, 30 μM AcLEHD-AFC for Casp9, and 50 μM AcIETD-AFC for Casp10) was added for a total assay volume of 20 μL/well. Fluorescence from free AFC was read at 37 °C at 10 time points over 40 min using a CLARIOstar plate reader (BMG Labtech) (λ_{ex} = 400 nm λ_{em} = 505 nm). The 21 min time point was considered for the assessment of inhibition reported as pIC_{50} and the ensuing pK_i value since progress curves of the corresponding reference inhibitors for each caspase confirmed linear product formation over a period of 25 min (Figure S203, Supporting Information; deviation from linearity was assessed considering Runs test and the R squared values of the simple linear regression fit). Concentration−response curves of the standard inhibitors (Figure S204, Supporting Information) and compounds **25**, **32**, **33**, and **47** (Figure S205, Supporting Information) show no dependence of the pIC_{50} values on the readout time point. Comparison of fluorometric cpCasp2 assay results at 0, 5, 15, and 30 min preincubation time for selected inhibitors (**1**, **25**, **32**, **33**, **47**, and **55**) is shown in Figure S206 in the Supporting Information. Evaluation of representative inhibitors (**1**, **25**, **32**, **33**, and **47**) at DTT concentrations ranging from 0.01 to 100 mM confirmed that 10 mM DTT provides optimal assay performance by maintaining maximal enzyme activity while minimizing effects on inhibitor potency (Figure S208, Supporting Information).

Jump Dilution Assay. The reference compounds emricasan and AcVDVAD-CHO and inhibitors **25**, **32**, **33**, and **47** were incubated in a concentration corresponding to 10 × IC_{50} with 10 nM cpCasp2 at 37 °C for 30 min in aqueous Casp2 assay buffer containing 100 mM MES (pH 6.5), 150 mM NaCl, 0.1% CHAPS, 1.5% sucrose, and 10 mM freshly added dithiothreitol (DTT). After incubation, the enzyme−inhibitor mixture was diluted 1:100 in assay buffer containing the substrate Z-VDVAD-AFC to a final concentration of 0.1 nM cpCasp2, 0.1 x IC_{50} of the inhibitor, and 10 μM AcVDVAD-AFC. Residual enzyme activity was measured at a CLARIOstar plate reader (BMG Labtech) at λ_{ex} = 400 nm and λ_{em} = 505 nm over 60 min. The residence time τ was defined as the reciprocal of the dissociation constant k_{off} of the binary enzyme−inhibitor complex and was calculated as described in the literature using the following equation: $[P] = v_s * t + (v_i - v_s)*(1-e^{-koff*t})/k_{off}$, where $[P]$ is the concentration of the product formed by substrate cleavage, v_s is the steady-state velocity of enzyme activity (expected to be 0.9091 × v_0), and v_i is the initial velocity (expected to be 0.091 × v_0), with v_0 representing the velocity of the uninhibited control sample (positive ctrl).[42] Mean residence times were calculated from at least three independent experiments, each performed in duplicate. The progress curves and calculated residence times are shown in Figure S210.

In Vitro Casp2-Catalyzed au Cleavage Assay

Procedure. Purified recombinant Casp2 was subjected to an extensive preincubation period to ensure binding with the inhibitory compounds. The enzyme, at a final concentration of 67 μM during this phase, was mixed with various test concentrations of the compounds. This mixture was kept at 4 °C for 90 h. Following this, the pretreated enzyme was introduced to purified recombinant full-length Tau at a 1:1 molar ratio in a 1x reaction buffer (25 mM HEPES, pH 7.5; 0.1% (w/v) CHAPS; 10 mM DTT) to start the cleavage reaction. The reaction was incubated at 37 °C for 6 h and then instantaneously terminated by adding 0.1% (v/v) protease inhibitor cocktail. The cleavage product Δtau314 is a 276-amino-acid protein consisting of a 20-amino-acid N-terminal tag followed by the 256-amino-acid tau fragment generated by Casp2 cleavage of full-length human 0N4R tau (383 amino acids). Under SDS-PAGE and WB, Δtau314 migrates with an apparent molecular weight of ∼37 kDa.

Immunoprecipitation/Western Blotting. Immunoprecipitation was conducted according to a previously published protocol.[15] Briefly, after the Casp2 cleavage reaction was terminated, the enzyme and cleavage products were diluted into 400 μL of immunoprecipitation (IP) buffer (50 mM Tris-HCl, pH 7.4; 150 mM NaCl, 0.1 mM phenylmethylsulfonyl fluoride, 0.2 mM 1,10-phenanthroline monohydrate, and a protease inhibitor cocktail (MilliporeSigma)). Next, this diluted mixture was incubated for 14−16 h at 4 °C with 10 μg of Δtau314-specific monoclonal antibody 4F3 and 50 μL of Protein G Sepharose 4 Fast Flow resin (GE Healthcare). Following this overnight incubation, the resin was extensively washed to remove non-specifically bound proteins, and the precipitated proteins were eluted from the resin. Finally, western blotting (WB) analysis was performed on the eluted material using biotin-conjugated 4F3 based on a protocol detailed in a prior publication to visualize and quantify the resulting cleavage products.[17] The levels of proteins were determined from two independent experiments.

In Vitro ADME Studies for MUR-65 (3). In vitro ADME of MUR-65 (**3**) was conducted by Cyprotex Discovery Ltd (Framingham, US), according to the protocols as described in the following sections.

Downloaded from pubs.acs.org/jmcmar/article-pdf/doi/10.1021/acs.jmedchem.6c01370/6911434/jm6c01370.pdf by UNIV REGENSBURG user on 17 November 2026

https://doi.org/10.1021/acs.jmedchem.6c01370
J. Med. Chem. XXXX, XXX, XXX−XXX

Kinetic Solubility in PBS (pH 7.4). 30 μL of MUR-65 (**3**, 10 mM in DMSO) and the positive control progesterone (30 mM in DMSO) were added to 970 μL of PBS (pH 7.4) in a 96-well rack. The vials were sealed and incubated at room temperature for 2 h while being shaken at 1100 rpm using a magnetic stir bar. After incubation, stir bars were removed, and the samples were transferred to a second filter plate and filtered using a Vacuum Manifold. 10 μL of the filtrate was diluted with 980 μL of acetonitrile and 10 μL of DMSO and quantified against 3 μM standards (STD) on LC/MS/MS analysis. For preparation of the standards, a 10 mM compound stock solution was diluted with DMSO to 300 μM of which 10 μL was diluted with 980 μL of acetonitrile and 10 μL of PBS (pH 7.4). LC/MS/MS analysis was performed on a Shimadzu Triple Quad™ 5500 instrument from AB Inc (Canada) equipped with an ESI interface using an XSelect™ HSS T3 XP column (100 Å, 2.5 μm, 2.1 × 30 mm; Waters, Milford, USA) as the stationary phase (tempered to 40 °C) and 0.1% formic acid in water and 0.1% formic acid in acetonitrile with a flow rate of 1 mL/min as the mobile phase. MS/MS analysis was setup in positive multiple reaction monitoring (MRM^+) mode at 500 °C with an ionspray voltage of 5500 V. The study was performed in duplicate, and the solubility of the test compound in the sample was calculated from $[\text{sample}] = (A_{\text{sample}} * V_{\text{STD}} * DF_{\text{sample}} * [\text{STD}])/(A_{\text{STD}} * V_{\text{sample}})$, where A is the peak area, V is the injection volume (3 μL), and DF is the dilution factor. Any value close to or above 300 μM indicates that the compound may have a solubility at or above 300 μM. The solubility was determined to be 277.17 μM for MUR-65 and 19.91 μM for progesterone.

LogD. 15 μL of MUR-65 (**3**, 1 mM in DMSO) or the control compound progesterone (10 mM in DMSO) was placed into a 96-well deep well plate. After adding 500 μL of phosphate buffer (pH 7.4)-saturated 1-octanol, the plate was vortexed for 2 min at 1000 rpm, followed by the addition of 500 μL of 1-octanol-saturated phosphate buffer. The plate was then sealed and shaken at 2000 rpm at 25 °C for 2 h using an Eppendorf Thermomixer Comfort plate shaker. Afterward, the plate was centrifuged for 30 min at 25 °C and 3,220*g* to separate the phases. 50 μL of aliquots from the upper (1-octanol) and lower (buffer) phases were diluted with 450 μL of acetonitrile containing the internal standards labetalol, tolbutamide, and ketoprofen. Several dilution steps including the addition of the respective opposite phase were carried out to achieve appropriate peak shape and size for subsequent quantification via LC/MS/MS analysis, which was performed on a Shimadzu Triple Quad™ 6500 instrument from AB Inc (Canada) equipped with an ESI interface using an XSelect™ HSS T3 XP column (100 Å, 2.5 μm, 2.1 × 50 mm; Waters, Milford, USA) as the stationary phase (tempered to 40 °C) and 0.1% formic acid in water and 0.1% formic acid in acetonitrile with a flow rate of 0.65 mL/min as the mobile phase. MS/MS analysis was setup in positive multiple reaction monitoring (MRM^+) mode at 500 °C with an ionspray voltage of 5500 V. The assay was performed in duplicate. The relative peak area of the test compound referred to the internal standard was determined from the extracted ion chromatogram and gives the LogD value as $\log D = \log(\text{Area ratio}_{\text{octanol phase}} * \text{DF}_{\text{octanol phase}}/\text{Area ratio}_{\text{buffer phase}} * \text{DF}_{\text{buffer phase}})$, where DF is the dilution factor. The logD of MUR-65 was calculated to be −1.81, and the logD of Progesterone was calculated to be 3.96.

Permeability in MDCK-MDR1 Cells. MDCK-MDR1 cells were cultured with Gibco Minimum Essential Media (MEM) containing FBS (AusGenex, City of Gold Coast, Australia), and penicillin/streptomycin (Solarbio, Beijing, China) for 3−8 days at 37 °C, 5% CO_2, and 95% relative humidity before the cells were seeded into 96-well HTS transwell plates (Corning, New York, USA). To assess the cell monolayer integrity, the transepithelial electrical resistance (TEER) across the monolayer was measured with a Millicell Epithelial Volt-Ohm measuring system (Millipore, USA) before performing the assay. A TEER value of >42 Ω•cm^2 was considered acceptable to indicate a well-qualified monolayer. 200 μM stock solutions of MUR-65 (**3**) and the positive controls metoprolol, prazosin, and imatinib in DMSO were diluted with HBSS (10 mM HEPES, pH 7.4) to get 1 μM working solutions. The final concentration of DMSO in the incubation system was 0.5%. To determine the rate of drug transport from the apical (A) to basolateral (B) compartments, 75 μL of the working solution of the test compound was added to the transwell insert (apical compartment), and the wells in the receiver plate (basolateral compartment) were filled with 235 μL of HBSS (10 mM HEPES, pH 7.4). To determine the rate of drug transport from the basolateral to apical compartment, 235 μL of the working solution of the test compound was added to the receiver plate wells, and the transwell inserts were filled with 75 μL of HBSS (10 mM HEPES, pH 7.4). After incubation for 2 h at 37 °C, 50 μL of samples from donor sides and receiver sides were transferred to wells of a new 96-well plate, followed by the addition of 200 μL of cold methanol containing appropriate internal standards. The samples were vortexed for 5 min and centrifuged at 3,220*g* for 40 min 100 μL of the supernatant was diluted with water and analyzed via LC−MS/MS on a Shimadzu Triple Quad™ 5500 instrument from AB Inc (Canada) equipped with an ESI interface using an XSelect™ HSS T3 XP column (100 Å, 2.5 μm, 2.1 × 30 mm; Waters, Milford, USA) as the stationary phase (tempered to 40 °C) and 0.1% formic acid in water and 0.1% formic acid in acetonitrile with a flow rate of 1 mL/min as the mobile phase. MS/MS analysis was setup in positive multiple reaction monitoring (MRM^+) mode at 500 °C with an ionspray voltage of 5500 V. The assay was performed in duplicate. The leakage after 2 h of the transport period was determined by adding Lucifer Yellow (LY) to a final concentration of 100 μM to the apical compartment. After incubation for 30 min at 37 °C, 80 μL of aliquots were sampled from the apical and basolateral compartments, and the LY fluorescence signal was measured at 485 nm excitation and 530 nm emission. An LY leakage of <1% was considered acceptable to indicate a well-qualified MDCK-MDR1 monolayer. The apparent permeability coefficient P_{app} was calculated as $P_{\text{app}} = (V_A \times [\text{drug}]_{\text{acceptor}})/(\text{Area} \times t \times [\text{drug}]_{\text{initial, donor}})$, where V_A is the volume in the acceptor well (mL), Area is the surface area of the membrane (0.143 cm^2), and t is the total transport time (s). The efflux ratio was calculated as Efflux Ratio = $P_{\text{app}}(\text{B-A})/P_{\text{app}}(A\text{-}B)$, and the recovery was calculated as $\text{Rec\%} = (V_A \times [\text{drug}]_{\text{acceptor}} + V_D \times [\text{drug}]_{\text{donor}})/(V_D \times [\text{drug}]_{\text{initial, donor}})$, where V_A is the volume (mL) in the acceptor well and V_D is the volume (mL) in the donor well. The results are summarized in Table S3.

Stability in Human and Mouse Plasma and Blood. Pooled, gender-mixed human plasma and blood (K_2EDTA) from healthy Asian volunteers was collected in a domestic hospital with ethical approval and was purchased from a local vendor. Pooled, gender-mixed mouse plasma and blood (K_2EDTA) from CD-1 mice were purchased from BioIVT LCC (Westbury, USA) and SPFBiotechnology Co. (Bejing, China), respectively. 1 mM working stock solutions of MUR-65 (**3**) (in DMSO) and the positive control propantheline (in acetonitrile) were spiked to pre-incubated plasma/whole blood to reach a final concentration of 5 μM and a final solvent concentration of 0.5%. 50 μL aliquots of the spiked plasma/whole blood were incubated at 37 °C while shaking at 60 rpm. At appointed timepoints of 0 min, 15 min, 30 min, 60 min, and 120 min of incubation, the reaction was stopped by adding 300 μL of room-temperature quench solution (acetonitrile with 3% formic acid containing internal standards alprazolam, labetalol, and ketoprofen) to the samples. After vortexing for 5 min, the precipitated protein was separated by centrifugation at 4 °C and 3,220 *g* for 30 min 100 μL of the supernatant was diluted with 100 μL of water and quantified via LC−MS/MS analysis on a Shimadzu Triple Quad™ 6500 instrument (plasma samples) or a Shimadzu Triple Quad™ 4500 instrument (for blood samples) both from AB Inc (Canada) equipped with an ESI interface using an XSelect™ HSS T3 XP column (100 Å, 2.5 μm, 2.1 × 50 mm; Waters, Milford, USA) as the stationary phase (tempered to 40 °C) and 0.1% formic acid in water and 0.1% formic acid in acetonitrile with a flow rate of 1 mL/min as the mobile phase. MS/MS analysis was setup in positive multiple reaction monitoring (MRM^+) mode at 550 °C with an ionspray voltage of 5500 V. The relative peak area of the test compound referred to the internal standard was determined from the extracted ion chromatogram and gives the percentage of the remaining compound as the ratio of the relative peak area at the respective timepoint and the relative peak area at a timepoint

Downloaded from pubs.acs.org/jmcmar/article-pdf/doi/10.1021/acs.jmedchem.6c01370/6911434O/jm6c01370.pdf by UNIV REGENSBURG user on 17 November 2026

https://doi.org/10.1021/acs.jmedchem.6c01370
J. Med. Chem. XXXX, XXX, XXX−XXX

of 0 min. The slope value k was obtained by the linear fit of the natural logarithm of remaining percentage plotted against incubation time. The in vitro half-life (in vitro $t_{1/2}$) was determined from the slope value as in vitro $t_{1/2} = -0.693/k$. The results are summarized in Figures 4A and S5A.

Plasma Protein Binding. Pooled, gender-mixed human plasma and blood (K_2EDTA) from healthy Asian volunteers were collected in a domestic hospital with ethical approval and was purchased from a local vendor. Pooled, gender-mixed mouse plasma and blood (K_2EDTA) from CD-1 mice were purchased from BioIVT LCC (Westbury, US) and SPFBiotechnology Co. (Bejing, China), respectively. 200 μM working stock solutions of MUR-65 (**3**) and the positive control ketoconazole in DMSO were spiked to pre-incubated plasma/whole blood to reach a final concentration of 1 μM and a final solvent concentration of 0.5%. After membrane dialysis against PBS for 6 h at 37 °C, 50 μL of aliquots from both buffer and plasma chambers were added to 400 μL of quench solution (acetonitrile containing internal standards labetalol, tolbutamide, and ketoprofen). After vortexing for 2 min and centrifugation at 3,220g for 30 min, 100 μL of the supernatant was diluted with 100 μL of water, and the mixture was analyzed via LC−MS/MS on a Shimadzu Triple Quad™ 6500 instrument from AB Inc (Canada) equipped with an ESI interface using an XSelect™ HSS T3 XP column (100 Å, 2.5 μm, 2.1 × 50 mm; Waters, Milford, USA) as the stationary phase (tempered to 40 °C) and 0.1% formic acid in water and 0.1% formic acid in acetonitrile with a flow rate of 0.65 mL/min as the mobile phase. MS/MS analysis was setup in positive multiple reaction monitoring (MRM^+) mode at 500 °C with an ionspray voltage of 5500 V. The assay was performed in duplicate, and the concentrations of the test compound in buffer and plasma chambers were determined from the peak area ratio referred to the internal standards. The percentage of the bound compound was calculated as follows: % bound = 100%—% free with % free = (Peak Area Ratio$_{\text{buffer chamber}}$/Peak Area Ratio$_{\text{plasma chamber}}$) *100%; % recovery = (Peak Area Ratio$_{\text{buffer chamber}}$ + Peak Area Ratio $_{\text{plasma chamber}}$)/Peak Area Ratio$_{\text{total sample}}$*100%; % stability = Peak Area Ratio$_{\text{6h sample}}$/Peak Area Ratio$_{\text{0 h sample}}$*100%. The results are summarized in Figure S5B.

Metabolic Stability in Human and Mouse Hepatocytes. Cryopreserved human hepatocytes were purchased from BioIVT (New York, USA); cryopreserved male ICR/CD-1 mouse hepatocytes were purchased from Milecell Bio (Sugarland, USA). Upon thawing, a portion of the cell suspension was boiled for 5 min to serve as a negative control. Both viable and boiled hepatocytes were placed in a 96-well plate to a cell density of 0.1 × 10^6 cells/well and pre-incubated for 10 min before MUR-65 (**3**) and the positive control verapamil were added from 10 mM stock solutions in DMSO to a final concentration of 1 μM and a final DMSO concentration of 0.01%. At designated timepoints of 0 min, 15 min, 30 min, 60 min, 90 min, and 120 min of incubation at 37 °C, 25 μL of aliquots were quenched with 150 μL of cold acetonitrile containing the internal standards tolbutamide, ketoprofen, labetalol, caffeine, and diclofenac. After centrifugation for 45 min at 3,220g, 100 μL of the supernatant was diluted by 100 μL of water and analyzed via LC/MS/MS on a Shimadzu Triple Quad™ 6500 instrument from AB Inc (Canada) equipped with an ESI interface using an XSelect™ HSS T3 XP column (100 Å, 2.5 μm, 2.1 × 50 mm; Waters, Milford, USA) as the stationary phase (tempered to 40 °C) and 0.1% formic acid in water and 0.1% formic acid in acetonitrile with a flow rate of 0.65 mL/min as the mobile phase. MS/MS analysis was setup in positive multiple reaction monitoring (MRM^+) mode at 500 °C with an ionspray voltage of 5500 V. The assay was performed in duplicate, and negative controls were prepared in singlicate. The relative peak area of the test compound referred to the internal standard was determined from the extracted ion chromatogram and gives the percentage of the remaining compound as the ratio of the relative peak area at the respective timepoint and the relative peak area at a timepoint of 0 min. The slope value k was obtained by the linear fit of the natural logarithm of remaining percentage plotted against incubation time. The in vitro half-life (in vitro $t_{1/2}$) was determined from the slope value as in vitro $t_{1/2} = -0.693/k$. The in vitro intrinsic clearance, in vitro CL_{int}, was calculated from in vitro $CL_{int} = k*V/N$, where V is the incubation volume (0.2 mL) and N is the number of hepatocytes per well (0.1 × 10^6 cells). The results are summarized in Figure S6A,D.

Metabolic Stability in Human and Mouse Liver S9 Fractions. Gender pooled human and male CD-1 mouse liver S9 fractions were purchased from Xenotech (Kansas City, USA) and placed in a 96-well plate to a final concentration of 1 mg/mL together with 5 mM $MgCl_2$, 100 mM phosphate buffer, and 1 mM NADPH. Negative control samples were prepared by replacing NADPH with water. The mixture was warmed for 5 min at 37 °C before the reaction was started by adding MUR-65 (**3**) or the positive control verapamil from a 10 mM DMSO stock solution to each well (final compound concentration of 1 μM, final DMSO concentration of 0.1%). At designated timepoints of 0, 15, 45, and 60 min of incubation at 37 °C, 50 μL aliquots were quenched with 200 μL of cold methanol containing the internal standards imipramine, labetalol, and ketoprofen. After centrifugation for 40 min at 3,220g, 90 μL of the supernatant was diluted by 90 μL of water and analyzed via LC/MS/MS on a QTRAP 4500 instrument from Sciex (Toronto, Canada) equipped with an ESI interface using an XSelect™ HSS T3 XP column (100 Å, 2.5 μm, 2.1 × 30 mm; Waters, Milford, USA) as the stationary phase (tempered to 40 °C) and 0.1% formic acid in water and 0.1% formic acid in acetonitrile with a flow rate of 1 mL/min as the mobile phase. MS/MS analysis was setup in positive multiple reaction monitoring (MRM^+) mode at 500 °C with an ionspray voltage of 5500 V. The assay was performed in duplicate, and negative controls were prepared in singlicate. The relative peak area of the test compound referred to the internal standard was determined from the extracted ion chromatogram and gives the percentage of the remaining compound as the ratio of the relative peak area at the respective timepoint and the relative peak area at a timepoint of 0 min. The slope value k was obtained by the linear fit of the natural logarithm of remaining percentage plotted against incubation time. The in vitro half-life (in vitro $t_{1/2}$) was determined from the slope value as in vitro $t_{1/2} = -0.693/k$. The in vitro intrinsic clearance, in vitro CL_{int}, was calculated as in vitro $CL_{int} = k*V/m$, where V is the incubation volume (0.4 mL) and m is the amount of protein per well (mg). The results are summarized in Figure S6B, D.

Metabolic Stability in Human and Mouse Liver Microsomes. Pooled male and female liver microsomes were purchased from Discovery Life Science (Huntsville, USA); pooled male CD-1 mouse liver microsomes were purchased from Xenotech (Kansas City, USA). The microsomes were placed in a 96-well plate to a final assay concentration of 0.56 mg/mL together with 111 mM phosphate buffer. 1 mM DMSO stock solutions of MUR-65 (**3**) and the positive control verapamil were added to a final compound concentration of 1 μM and a final DMSO concentration of 0.1%. The mixture was warmed for 5 min at 37 °C before the reaction was started by adding the NADPH solution to a final assay concentration of 1 mM. Negative control samples were prepared by replacing NADPH with water. At designated timepoints of 0, 15, 45, and 60 min of incubation at 37 °C, 10 μL of aliquots were quenched with 120 μL of cold acetonitrile containing the internal standards tolbutamide, llabetelol, and ketoprofen. After centrifugation of the samples for 45 min at 3,220g, 40 μL of the supernatant was diluted by 40 μL of water and analyzed via LC/MS/MS on a Triple Quad™ 6500$^+$ instrument from Sciex (Toronto, Canada) equipped with an ESI interface using an XSelect™ HSS T3 XP column (100 Å, 2.5 μm, 2.1 × 30 mm; Waters, Milford, USA) as the stationary phase (tempered to 40 °C) and 0.1% formic acid in water and 0.1% formic acid in acetonitrile with a flow rate of 0.65 mL/min as the mobile phase. MS/MS analysis was set up in positive multiple reaction monitoring (MRM^+) mode at 500 °C with an ionspray voltage of 5500 V. The assay was performed in duplicate, and negative controls were prepared in singlicate. The relative peak area of the test compound referred to the internal standard was determined from the extracted ion chromatogram and gives the percentage of the remaining compound as the ratio of the relative peak area at the respective timepoint and the relative peak area at a timepoint of 0 min. The slope value k was obtained by the linear fit of the natural logarithm of remaining percentage plotted against

Downloaded from pubs.acs.org/jmcmar/article-pdf/doi/10.1021/acs.jmedchem.6c01370/6911434/jm6c01370.pdf by UNIV REGENSBURG user on 17 November 2026

https://doi.org/10.1021/acs.jmedchem.6c01370
J. Med. Chem. XXXX, XXX, XXX−XXX

incubation time. The in vitro half-life (in vitro $t_{1/2}$) was determined from the slope value as in vitro $t_{1/2} = -0.693/k$. The in vitro intrinsic clearance, in vitro CL_{int}, was calculated as in vitro $CL_{int} = k*V/m$, where V is the incubation volume (0.4 mL) and m is the amount of protein per well (mg).

In Vivo Pharmacokinetic Study of MUR-65 in CD-1 Mice. In vivo PK studies of MUR-65 (**3**) were conducted by Pharmaron Co. Ltd. (Beijing, China) according to the protocols described in the following.

All procedures related to animal handling, care, and the treatment in this study are performed according to the Animal care and Use Protocol (AUP, PK-M-07182024) approved by the Institutional Animal Care and Use Committee (IACUC) of Pharmaron following the guidance of the Association for Assessment and Accreditation of Laboratory Animal Care (AAALAC). Pharmaron's IACUC policies follow laws and regulations of local government for animal research and are in compliance with the guidelines of the Guide for the Care and Use of Laboratory Animals ("The Guide"). Pharmaron adheres to the "3R" principle (Replacement, Reduction, and Refinement) for animal welfare management.

For the determination of in vivo pharmacokinetics in plasma and brain tissue, MUR-65 (**3**) was administered via an intracerebroventricular (icv) injection of 1 mg/kg and via a subcutaneous injection of 1 mg/kg and 10 mg/kg to male and female CD-1 mice (obtained from SPF Biotechnology Co., Ltd., Beijing, CH). The study was designed in triplicate, meaning that brain and plasma samples of three individual animals for every sex, dose, and administration route were collected at timepoints of 0.5 h, 1 h, 2 h, 4 h, 8 h, 12 h, and 24 h post dosing. A total of 154 animals (male and female) were treated. The formulations were prepared based on the TFA salt of MUR-65 (molecular weight 791.78 Da), which was dissolved for icv formulation in 100% DMSO to a concentration of 3 mg/mL and for sc formulation in DMSO/PBS 10/90 to a concentration of 0.2 mg/mL and 2 mg/mL (for 1 mg/ml and 10 mg/ml dose, respectively). Brain samples were prepared for homogenization by adding deionized water in a ratio of 1:4 (m/m). 45 μL of aliquots of brain homogenates and plasma samples were added to 150 μL of acetonitrile containing the internal standard carbamazepine. After vortexing for 30 s and centrifugation at 4 °C and 4000 rpm for 15 min, the supernatant was quantified on LC/MS/MS based on a nine-point calibration curve of standards, which was prepared separately for brain and plasma samples by spiking mouse blank plasma and mouse blank brain homogenate with MUR-65 to the final concentrations of 0.5, 1, 2, 5, 10, 50, 100, 500, and 1000 ng/mL. Five quality control samples at 1.5 ng/mL, 3 ng/mL, 6 ng/mL, 160 ng/mL, and 800 ng/mL for both brain and plasma samples were prepared on the day of analysis independently of those used for the calibration curves. LC/MS/MS analysis was performed using a Shimadzu Triple Quad^{TM} 6500^{+} instrument equipped with an ESI interface using a Phenomenex Synergi Polar-RP column (2.5 μm, 100 Å, 50 × 3.0 mm, Phenomenex Ltd., Aschaffenburg, Germany) as the stationary phase and 95% water with 10 mM ammonium acetate (A) and 95% acetonitrile with 10 mM ammonium acetate (B) as the mobile phase. A linear gradient A:B of 0 min: 100:0, 0.3–2.5 min: 0:100, 2.5–2.7 min: 0:100 and 2.7–3 min: 100:0 and a flow rate of 0.6 mL/min were applied. The plot of the concentration in plasma and brain samples against the time gives the area under curve (AUC_{last_plasma} and AUC_{last_brain}) and subsequent the brain plasma ratio as $AUC_{last_brain}/AUC_{last_plasma}$. The slope value k was obtained by the linear fit of the natural logarithm of the concentration against time. The plasma and brain half-life ($t_{1/2_plasma}$ and $t_{1/2_brain}$) were determined from the slope value as $t_{1/2} = -0.693/k$. The limit of quantification was 1 ng/mL for plasma and 5 ng/g for brain samples. PK parameters were estimated by the non-compartmental model with the calculation model of "Linear up log down" using WinNonlin 8.3.1.

Crystallography

The recombinant protein was prepared and purified as previously described.[27] The ligand–protein complex was obtained by cocrystallization using an Art Robbins Pheonix liquid handler. The plates were automatically imaged with a JANSi imager UVEX. Crystals suitable for X-ray diffraction were harvested, and data were collected at the NSLSII 17-ID-1 beamline (Long island, NY). Datasets were processed with XDS.[43] The structure was solved by molecular replacement with phaser[44] using PDB ID 8VP4 as the search model. Iterative refinement and modeling building were done using the PHENIX[45] suite and COOT.[46] A clear electron density map ($2F_o$-F_c) as well as the Fo–Fc omit map corresponding to the ligand enabled unambiguous placement in the active site. Crystallographic statistics are summarized in Table S6 in the Supporting Information, and the final coordinates and structure factors have been deposited in the Protein Data Bank under accession code 9ZEW and 9ZEX, respectively.

Data Analysis

Statistical analyses were performed using GraphPad Prism version 10 (GraphPad Software, La Jolla, CA). IC_{50} values were obtaied by fitting the dose–response data with four-parameter variable slope nonlinear regression. These were transformed into pK_i values using the Cheng–Prusoff equation ($K_i = IC_{50}/(1 + [S]/K_M)$).[47] Because the compounds are covalent-reversible inhibitors, they were characterized using pK_i values and not "k_{inact}/K_I", as would be necessary for covalent irreversible inhibitors. $P < 0.05$ was considered statistically significant. Hill slopes of selected compounds (**1**, **25**, **32**, **33**, and **47**) in the fluorometric cpCasp2 assay are shown in Table S13 (Supporting Information).

■ ASSOCIATED CONTENT

Supporting Information

The Supporting Information is available free of charge at https://pubs.acs.org/doi/10.1021/acs.jmedchem.6c01370.

CNS MPO scores (Table S1), RP-HPLC stability control of compounds **27** and **28** (Figures S1–S4), ADME profiling of compound **3** (MUR-65) (Tables S2 and S3 and Figures S5 and S6), chemical structures of unnatural amino acids (Table S5) and compounds **1**–**55** (Figures S7–S61), NMR spectra of building blocks **BB1**–**BB4** (Figures S62–S69), NMR spectra of final compounds **8**–**55** (Figures S70–S151), RP-HPLC chromatograms of final compounds **8**–**55** (Figures S152–S199), crystallography (Figures S200–S202 and Tables S6–S11), experimental details for the synthesis of **BB1**–**BB4**, **8**–**31**, **34**–**46**, and **48**–**55** (Scheme S1), and fluorometric caspase assay (Figures S203–S209 and Tables S12 and S13) (PDF)

Molecular formula strings of compounds **1**–**55** (CSV)

Accession Codes

Atomic coordinates and reflection data for crystallographic complexes of JF1cpCasp2 with AcVDV(Dab)D-CHO (**2**, PDB ID: 9ZEW) and Idc(hE)G((*S*)-Me-THIQ)D-CHO (**33**, PDB ID: 9ZEX) have been deposited into the Protein Data Bank. The authors will release the atomic coordinates upon article publication.

■ AUTHOR INFORMATION

Corresponding Authors

Michael A. Walters – *Department of Medicinal Chemistry, Institute for Therapeutics Discovery and Development, University of Minnesota, Minneapolis, Minnesota 55414, USA;* orcid.org/0000-0001-5650-9277; Email: mwalters@umn.edu

Downloaded from pubs.acs.org/jmcmar/article-pdf/doi/10.1021/acs.jmedchem.6c01370/6911434/jm6c01370.pdf by UNIV REGENSBURG user on 17 November 2026

Steffen Pockes − *Department of Pharmaceutical and Medicinal Chemistry, Institute of Pharmacy, University of Regensburg, Universitätsstraße 31 93053, Regensburg, Germany;* orcid.org/0000-0002-2211-9868; Email: steffen.pockes@ur.de

Authors

Lisa Forster − *Department of Pharmaceutical and Medicinal Chemistry, Institute of Pharmacy, University of Regensburg, Universitätsstraße 31 93053, Regensburg, Germany*

Bernadette Vallaster − *Department of Pharmaceutical and Medicinal Chemistry, Institute of Pharmacy, University of Regensburg, Universitätsstraße 31 93053, Regensburg, Germany*

Alexander Hubmann − *Department of Pharmaceutical and Medicinal Chemistry, Institute of Pharmacy, University of Regensburg, Universitätsstraße 31 93053, Regensburg, Germany*

Merlin Bresinsky − *Department of Pharmaceutical and Medicinal Chemistry, Institute of Pharmacy, University of Regensburg, Universitätsstraße 31 93053, Regensburg, Germany*

Jessica L. Fuller − *Department of Medicinal Chemistry, Institute for Therapeutics Discovery and Development, University of Minnesota, Minneapolis, Minnesota 55414, USA*

Ke Shi − *College of Biological Sciences, University of Minnesota, Nanoliter Crystallization Facility, Minneapolis, MN 55455, USA;* orcid.org/0000-0003-4175-3714

Ian P. Lapcinski − *Department of Neurology, University of Minnesota, 2101 6th Street SE, Minneapolis 55455, USA*

Peng Liu − *Department of Neurology, University of Minnesota, 2101 6th Street SE, Minneapolis 55455, USA;* orcid.org/0000-0003-2615-1213

Mu Yang − *Department of Medicinal Chemistry, Institute for Therapeutics Discovery and Development, University of Minnesota, Minneapolis, Minnesota 55414, USA;* orcid.org/0000-0002-3041-8235

Jessica M. Strasser − *Department of Medicinal Chemistry, Institute for Therapeutics Discovery and Development, University of Minnesota, Minneapolis, Minnesota 55414, USA*

Kathryn M. Nelson − *Department of Medicinal Chemistry, Institute for Therapeutics Discovery and Development, University of Minnesota, Minneapolis, Minnesota 55414, USA*

Kristen John − *Department of Medicinal Chemistry, Institute for Therapeutics Discovery and Development, University of Minnesota, Minneapolis, Minnesota 55414, USA;* orcid.org/0000-0002-9981-6100

Deepti Mudaliar − *Department of Medicinal Chemistry, Institute for Therapeutics Discovery and Development, University of Minnesota, Minneapolis, Minnesota 55414, USA*

Lukas Wirth − *Department of Pharmaceutical and Medicinal Chemistry, Institute of Pharmacy, University of Regensburg, Universitätsstraße 31 93053, Regensburg, Germany*

Jonas Daschner − *Department of Pharmaceutical and Medicinal Chemistry, Institute of Pharmacy, University of Regensburg, Universitätsstraße 31 93053, Regensburg, Germany*

Herwig Pongratz − *Department of Pharmaceutical and Medicinal Chemistry, Institute of Pharmacy, University of Regensburg, Universitätsstraße 31 93053, Regensburg, Germany*

Karen H. Ashe − *Department of Neurology, University of Minnesota, 2101 6th Street SE, Minneapolis 55455, USA*

Complete contact information is available at: https://pubs.acs.org/doi/10.1021/acs.jmedchem.6c01370

Author Contributions

[⊥]L.F. and B.V. contributed equally to this work. The manuscript was written through contributions of all authors. All authors have given approval to the final version of the manuscript. K.H.A., M.A.W., and S.P.: resources; M.A.W. and S.P.: conceptualization; L.F., B.V., A.H., M.B., J.L.F., K.S., I.P.L., P.L., M.Y., J.M.S., K.J., D.M., L.W., and J.D.: formal analysis; L.F., B.V., A.H., M.B., J.L.F., K.S., I.P.L., P.L., M.Y., J.M.S., K.M.N., K.J., D.M., L.W., and J.D.: investigation; L.F., B.V., M.B., K.S., P.L., and S.P.: writing—original draft; L.F., B.V., A.H., K.S., P.L., and S.P.: visualization; K.H.A., M.A.W., S.P.: funding acquisition; all authors: writing—review and editing; K.H.A., M.A.W., and S.P.: supervision; and M.A.W. and S.P.: project administration.

Funding

This work was funded by NIH grant R01AG062199 (Ashe, Walters; subaward Pockes) and Lucas Brothers Foundation (Caspase-2 Inhibitors to Reverse Cognitive Decline, Ashe). S.P. thanks the German Research Foundation DFG for research grant PO 2563/3−1 and Heisenberg professorship PO 2563/4−1. S.P. was also supported by the Fonds der Chemischen Industrie (No. 661688) and Alzheimer Forschung Initiative e.V. (AFI, International Training Grant for M.B.).

Notes

The authors declare the following competing financial interest(s): K.H.A., M.W.A., and S.P. are founders and shareholders of Myriel, Inc., which is developing caspase-2 inhibitors to treat Alzheimer's disease and related dementias. Current addresses: M.B.: Bionorica SE, Neumarkt, Germany; J.L.F., J.M.S., and K.M.N.: Bio-Techne Corporation, Minneapolis, MN, USA; I.P.L.: University of California Los Angeles, Los Angeles, CA, USA; L.W. Heidolph Scientific Products GmbH, Schwabach, Germany.

■ ACKNOWLEDGMENTS

This manuscript is the first of two back-to-back publications and is related to Vallaster et al.[48] The authors thank Vivien Czipper and Julia Blüml for excellent technical assistance. The TOC graphic was created with Biorender.com.

■ ABBREVIATIONS

AAALAC, Assessment and Accreditation of Laboratory Animal Care; Abz, para-aminobenzoic acid; AFC, 7-amino-4-trifluoromethylcoumarin; Ambz, para-aminomethylbenzoic acid; AVA, 5-aminovalerianic acid; AU, absorption units; AUP, Animal care and Use Protocol; BB, building block; BnT, O-benzyl-L-threonine; Casp1, caspase-1; Casp2, caspase-2; Casp3, caspase-3; Casp6, caspase-6; Casp7, caspase-7; Casp9, caspase-9; CHAPS, 3-[(3-cholamidopropyl)dimethylammonio]-1-propanesulfonate; CL, clearance; cmpd, compound; CNS MPO, central nervous system multiparameter

Downloaded from pubs.acs.org/jmcmar/article-pdf/doi/10.1021/acs.jmedchem.6c01370/6911434O/jm6c01370.pdf by UNIV REGENSBURG user on 17 November 2026

optimization; cpCasp2, circularly permutated caspase2; ctrl, control; Dab, diaminobutyric acid; DAD, diode array detector; DIPEA, N,N-diisopropylethylamine; D_2O, deuterium oxide; HATU, [O-(7-azabenzotriazol-1-yl)-N,N,N′,N′-tetramethyluronium-hexafluorphosphat]; HBSS, Hanks' balanced salt solution; HD, hHuntington's disease; hE, homoglutamic acid; HEPES, 4-(2-hydroxyethyl)-1-piperazinethanesulfonic acid; IACUC, Institutional Animal Care and Use Committee; Idc, S-indoline-2-carboxylic acid; Ind, indole-2-carboxylic acid; IP, immunoprecipitation; K_2EDTA, dipotassium ethylenediaminetetraacetic acid; LOQ, limit of quantification; MDCK, Madin−Darby Canine Kidney; MDR1, multidrug resistance protein1; MeCN, acetonitrile; MeOD, methanol-d4; MES, 2-(N-morpholino)ethanesulfonic acid; MRM+, multiple reaction monitoring; MWCO, molecular weight cutoff; PMSF, phenylmethylsulfonyl fluoride; PTFE, polytetrafluoroethylene; Quin, quinaldic acid; (R/S)-Br-THIQ, (R/S)-6-bromo-1,2,3,4-tetrahydroisoquinoline-1-carboxylic acid; (R/S)-Me-THIQ, (R/S)-6-methyl-1,2,3,4-tetrahydroisoquinoline-1-arboxylic acid; (R/S)-Me-THIQ*, (R/S)-5-fluoro-6-methyl-1,2,3,4-tetrahydroisoquinoline-1-carboxylic acid; RFU, relative fluorescent units; RP, reversed phase; SD, standard deviation; SEM, standard error of the mean; SI, Supporting Information; SI-HP, silica high-purity; SPPS, solid phase peptide synthesis; STD, standard; TEER, transepithelial electrical resistance; t_0, dead time; t_R, retention time; Tle, L-α-tert-leucine; TPSA, topological polar surface area; WB, Western blotting.

REFERENCES

(1) Yiannopoulou, K. G.; Papageorgiou, S. G. Current and Future Treatments for Alzheimer's Disease. *Ther. Adv. Neurol. Disord.* **2013**, *6* (1), 19−33.

(2) Herrmann, N.; Chau, S. A.; Kircanski, I.; Lanctôt, K. L. Current and Emerging Drug Treatment Options for Alzheimer's Disease: A Systematic Review. *Drugs* **2011**, *71* (15), 2031−2065.

(3) Fish, P. V.; Steadman, D.; Bayle, E. D.; Whiting, P. New Approaches for the Treatment of Alzheimer's Disease. *Bioorg. Med. Chem. Lett.* **2019**, *29* (2), 125−133.

(4) van Dyck, C. H.; Swanson, C. J.; Aisen, P.; Bateman, R. J.; Chen, C.; Gee, M.; Kanekiyo, M.; Li, D.; Reyderman, L.; Cohen, S.; Froelich, L.; Katayama, S.; Sabbagh, M.; Vellas, B.; Watson, D.; Dhadda, S.; Irizarry, M.; Kramer, L. D.; Iwatsubo, T. Lecanemab in Early Alzheimer's Disease. *N. Engl. J. Med.* **2023**, *388* (1), 9−21.

(5) Kwon, D. Debate Rages over Alzheimer's Drug Lecanemab as UK Limits Approval. *Nature* 2024.

(6) Vaz, M.; Silvestre, S. Alzheimer's Disease: Recent Treatment Strategies. *Eur. J. Pharmacol.* **2020**, *887*, 173554.

(7) Chong, F. P.; Ng, K. Y.; Koh, R. Y.; Chye, S. M. Tau Proteins and Tauopathies in Alzheimer's Disease. *Cell. Mol. Neurobiol.* **2018**, *38* (5), 965−980.

(8) Alonso, A. C.; Zaidi, T.; Grundke-Iqbal, I.; Iqbal, K. Role of Abnormally Phosphorylated Tau in the Breakdown of Microtubules in Alzheimer Disease. *Proc. Natl. Acad. Sci. U. S. A.* **1994**, *91* (12), 5562−5566.

(9) Teravskis, P. J.; Oxnard, B. R.; Miller, E. C.; Kemper, L.; Ashe, K. H.; Liao, D. Phosphorylation in Two Discrete Tau Domains Regulates a Stepwise Process Leading to Postsynaptic Dysfunction. *J. Physiol.* **2021**, *599* (9), 2483−2498.

(10) Santacruz, K.; Lewis, J.; Spires, T.; Paulson, J.; Kotilinek, L.; Ingelsson, M.; Guimaraes, A.; DeTure, M.; Ramsden, M.; McGowan, E.; et al. Tau Suppression in a Neurodegenerative Mouse Model Improves Memory Function. *Science* **2005**, *309* (5733), 476−481.

(11) Zhao, X.; Kotilinek, L. A.; Smith, B.; Hlynialuk, C.; Zahs, K.; Ramsden, M.; Cleary, J.; Ashe, K. H. Caspase-2 Cleavage of Tau Reversibly Impairs Memory. *Nat. Med.* **2016**, *22* (11), 1268−1276.

(12) Julien, O.; Wells, J. A. Caspases and Their Substrates. *Cell Death Differ.* **2017**, *24* (8), 1380−1389.

(13) Ramirez, M. L. G.; Salvesen, G. S. A Primer on Caspase Mechanisms. *Semin. Cell Dev. Biol.* **2018**, *82*, 79−85.

(14) Steuer, E. L.; Kemper, L. J.; Hlynialuk, C. J.; Leinonen-Wright, K.; Montonye, M. L.; Lapcinski, I. P.; Forster, C. L.; Ashe, K. H.; Liu, P. Blocking Site-Specific Cleavage of Human Tau Delays Progression of Disease-Related Phenotypes in Genetically Matched Tau-Transgenic Mice Modeling Frontotemporal Dementia. *J. Neurosci.* **2022**, *42*, 4737−4754.

(15) Liu, P.; Smith, B. R.; Montonye, M. L.; Kemper, L. J.; Leinonen-Wright, K.; Nelson, K. M.; Higgins, L.; Guerrero, C. R.; Markowski, T. W.; Zhao, X.; Petersen, A. J.; Knopman, D. S.; Petersen, R. C.; Ashe, K. H. A Soluble Truncated Tau Species Related to Cognitive Dysfunction Is Elevated in the Brain of Cognitively Impaired Human Individuals. *Sci. Rep.* **2020**, *10* (1), 3869.

(16) Smith, B. R.; Nelson, K. M.; Kemper, L. J.; Leinonen-Wright, K.; Petersen, A.; Keene, C. D.; Ashe, K. H. A Soluble Tau Fragment Generated by Caspase-2 Is Associated with Dementia in Lewy Body Disease. *Acta Neuropathol. Commun.* **2019**, *7* (1), 124.

(17) Liu, P.; Smith, B. R.; Huang, E. S.; Mahesh, A.; Vonsattel, J. P. G.; Petersen, A. J.; Gomez-Pastor, R.; Ashe, K. H. A Soluble Truncated Tau Species Related to Cognitive Dysfunction and Caspase-2 Is Elevated in the Brain of Huntington's Disease Patients. *Acta Neuropathol. Commun.* **2019**, *7* (1), 111.

(18) Schweizer, A.; Briand, C.; Grütter, M. G. Crystal Structure of Caspase-2, Apical Initiator of the Intrinsic Apoptotic Pathway. *J. Biol. Chem.* **2003**, *278* (43), 42441−42447.

(19) Poreba, M.; Salvesen, G. S.; Drag, M. Synthesis of a HyCoSuL Peptide Substrate Library to Dissect Protease Substrate Specificity. *Nat. Protoc.* **2017**, *12* (10), 2189−2214.

(20) Maillard, M. C.; Brookfield, F. A.; Courtney, S. M.; Eustache, F. M.; Gemkow, M. J.; Handel, R. K.; Johnson, L. C.; Johnson, P. D.; Kerry, M. A.; Krieger, F.; Meniconi, M.; Muñoz-Sanjuán, I.; Palfrey, J. J.; Park, H.; Schaertl, S.; Taylor, M. G.; Weddell, D.; Dominguez, C. Exploiting Differences in Caspase-2 and -3 S2 Subsites for Selectivity: Structure-Based Design, Solid-Phase Synthesis and in Vitro Activity of Novel Substrate-Based Caspase-2 Inhibitors. *Bioorg. Med. Chem.* **2011**, *19* (19), 5833−5851.

(21) Poreba, M.; Rut, W.; Groborz, K.; Snipas, S. J.; Salvesen, G. S.; Drag, M. Potent and Selective Caspase-2 Inhibitor Prevents MDM-2 Cleavage in Reversine-Treated Colon Cancer Cells. *Cell Death Differ.* **2019**, *26* (12), 2695−2709.

(22) Poreba, M.; Kasperkiewicz, P.; Snipas, S. J.; Fasci, D.; Salvesen, G. S.; Drag, M. Unnatural Amino Acids Increase Sensitivity and Provide for the Design of Highly Selective Caspase Substrates. *Cell Death Differ.* **2014**, *21* (9), 1482−1492.

(23) Fuentes-Prior, P.; Salvesen, G. S. The Protein Structures That Shape Caspase Activity, Specificity, Activation and Inhibition. *Biochem. J.* **2004**, *384* (2), 201−232.

(24) Chéreau, D.; Kodandapani, L.; Tomaselli, K. J.; Spada, A. P.; Wu, J. C. Structural and Functional Analysis of Caspase Active Sites. *Biochemistry* **2003**, *42* (14), 4151−4160.

(25) Bresinsky, M.; Strasser, J. M.; Vallaster, B.; Liu, P.; McCue, W. M.; Fuller, J.; Hubmann, A.; Singh, G.; Nelson, K. M.; Cuellar, M. E.; Wilmot, C. M.; Finzel, B. C.; Ashe, K. H.; Walters, M. A.; Pockes, S. Structure-Based Design and Biological Evaluation of Novel Caspase-2 Inhibitors Based on the Peptide AcVDVAD-CHO and the Caspase-2-Mediated Tau Cleavage Sequence YKPVD314. *ACS Pharmacol. Transl. Sci.* **2022**, *5* (1), 20−40.

(26) Singh, G.; Liu, P.; Yao, K. R.; Strasser, J. M.; Hlynialuk, C.; Leinonen-Wright, K.; Teravskis, P. J.; Choquette, J. M.; Ikramuddin, J.; Bresinsky, M.; Nelson, K. M.; Liao, D.; Ashe, K. H.; Walters, M. A.; Pockes, S. Caspase-2 Inhibitor Blocks Tau Truncation and Restores Excitatory Neurotransmission in Neurons Modeling FTDP-17 Tauopathy. *ACS Chem. Neurosci.* **2022**, *13* (10), 1549−1557.

Downloaded from pubs.acs.org/jmcmar/article-pdf/doi/10.1021/acs.jmedchem.6c01370/6911434/0/jm6c01370.pdf by UNIV REGENSBURG user on 17 November 2026

(27) Fuller, J. L.; Shi, K.; Pockes, S.; Finzel, B. C.; Ashe, K. H.; Walters, M. A. Reengineering of Circularly Permuted Caspase-2 to Enhance Enzyme Stability and Enable Crystallographic Studies. *ACS Chem. Biol.* **2025**, *20* (4), 845−857.
(28) Bresinsky, M.; Strasser, J. M.; Hubmann, A.; Vallaster, B.; McCue, W. M.; Fuller, J.; Singh, G.; Nelson, K. M.; Cuellar, M. E.; Finzel, B. C.; Ashe, K. H.; Walters, M. A.; Pockes, S. Characterization of Caspase-2 Inhibitors Based on Specific Sites of Caspase-2-Mediated Proteolysis. *Arch. Pharm. (Weinheim)* **2022**, *355* (9), e2200095.
(29) McStay, G. P.; Salvesen, G. S.; Green, D. R. Overlapping Cleavage Motif Selectivity of Caspases: Implications for Analysis of Apoptotic Pathways. *Cell Death Differ.* **2008**, *15* (2), 322−331.
(30) Lipinski, C. A.; Lombardo, F.; Dominy, B. W.; Feeney, P. J. Experimental and Computational Approaches to Estimate Solubility and Permeability in Drug Discovery and Development Settings. *Adv. Drug Deliv. Rev.* **1997**, *23* (1−3), 3−25.
(31) Wager, T. T.; Hou, X.; Verhoest, P. R.; Villalobos, A. Moving beyond Rules: The Development of a Central Nervous System Multiparameter Optimization (CNS MPO) Approach To Enable Alignment of Druglike Properties. *ACS Chem. Neurosci.* **2010**, *1* (6), 435−449.
(32) Chauvier, D.; Ankri, S.; Charriaut-Marlangue, C.; Casimir, R.; Jacotot, E. Broad-Spectrum Caspase Inhibitors: From Myth to Reality? *Cell Death Differ.* **2007**, *14* (2), 387−391.
(33) Chauvier, D.; Renolleau, S.; Holifanjaniaina, S.; Ankri, S.; Bezault, M.; Schwendimann, L.; Rousset, C.; Casimir, R.; Hoebeke, J.; Smirnova, M.; Debret, G.; Trichet, A.-P.; Carlsson, Y.; Wang, X.; Bernard, E.; Hébert, M.; Rauzier, J.-M.; Matecki, S.; Lacampagne, A.; Rustin, P.; Mariani, J.; Hagberg, H.; Gressens, P.; Charriaut-Marlangue, C.; Jacotot, E. Targeting Neonatal Ischemic Brain Injury with a Pentapeptide-Based Irreversible Caspase Inhibitor. *Cell Death Dis.* **2011**, *2* (9), e203.
(34) Bommarius, A. S.; Schwarm, M.; Drauz, K. Biocatalysis to Amino Acid-Based Chiral Pharmaceuticals—Examples and Perspectives. *J. Mol. Catal. B Enzym.* **1998**, *5* (1−4), 1−11.
(35) Franz, F.; Jechle, H.; Wilde, M.; Angerer, V.; Huppertz, L. M.; Longworth, M.; Kassiou, M.; Jung, M.; Auwärter, V. Structure-Metabolism Relationships of Valine and Tert-Leucine-Derived Synthetic Cannabinoid Receptor Agonists: A Systematic Comparison of the in Vitro Phase I Metabolism Using Pooled Human Liver Microsomes and High-Resolution Mass Spectrometry. *Forensic Toxicol.* **2019**, *37* (2), 316−329.
(36) Hanwell, M. D.; Curtis, D. E.; Lonie, D. C.; Vandermeersch, T.; Zurek, E.; Hutchison, G. R. A. An Advanced Semantic Chemical Editor, Visualization, and Analysis Platform. *J. Cheminformatics* **2012**, *4* (1), 17.
(37) Cserjan-Puschmann, M.; Lingg, N.; Engele, P.; Kröß, C.; Loibl, J.; Fischer, A.; Bacher, F.; Frank, A.-C.; Öhlknecht, C.; Brocard, C.; et al. Production of Circularly Permuted Caspase-2 for Affinity Fusion-Tag Removal: Cloning, Expression in Escherichia Coli, Purification, and Characterization. *Biomolecules* **2020**, *10* (12), 1592.
(38) Talanian, R. V.; Quinlan, C.; Trautz, S.; Hackett, M. C.; Mankovich, J. A.; Banach, D.; Ghayur, T.; Brady, K. D.; Wong, W. W. Substrate Specificities of Caspase Family Proteases. *J. Biol. Chem.* **1997**, *272* (15), 9677−9682.
(39) Pollastrini, M.; Lipparini, F.; Pasquinelli, L.; Balzano, F.; Barretta, G. U.; Pescitelli, G.; Angelici, G. A Proline Mimetic for the Design of New Stable Secondary Structures: Solvent-Dependent Amide Bond Isomerization of (*S*)-Indoline-2-Carboxylic Acid Derivatives. *J. Org. Chem.* **2021**, *86* (12), 7946−7954.
(40) Kim, K.; Kim, H. Y.; Oh, K. Aerobic Oxidation Approaches to Indole-3-Carboxylates: A Tandem Cross Coupling of Amines−Intramolecular Mannich−Oxidation Sequence. *Org. Lett.* **2019**, *21* (17), 6731−6735.
(41) Denault, J.-B.; Salvesen, G. S. Expression, Purification, and Characterization of Caspases. *Curr. Protoc. Protein Sci.* **2002**, *30* (1), 21.13. 1−21.13. 15.
(42) Copeland, R. A.; Basavapathruni, A.; Moyer, M.; Scott, M. P. Impact of Enzyme Concentration and Residence Time on Apparent Activity Recovery in Jump Dilution Analysis. *Anal. Biochem.* **2011**, *416* (2), 206−210.
(43) Kabsch, W. X. D. S. *XDS*. *Acta Crystallogr. D Biol. Crystallogr.* **2010**, *66* (2), 125−132.
(44) McCoy, A. J.; Grosse-Kunstleve, R. W.; Adams, P. D.; Winn, M. D.; Storoni, L. C.; Read, R. J. Phaser Crystallographic Software. *J. Appl. Crystallogr.* **2007**, *40* (4), 658−674.
(45) Adams, P. D.; Afonine, P. V.; Bunkóczi, G.; Chen, V. B.; Davis, I. W.; Echols, N.; Headd, J. J.; Hung, L.-W.; Kapral, G. J.; Grosse-Kunstleve, R. W.; et al. PHENIX: A Comprehensive Python-Based System for Macromolecular Structure Solution. *Acta Crystallogr. D Biol. Crystallogr.* **2010**, *66* (2), 213−221.
(46) Emsley, P.; Lohkamp, B.; Scott, W. G.; Cowtan, K. Features and Development of Coot. *Acta Crystallogr. D Biol. Crystallogr.* **2010**, *66* (4), 486−501.
(47) Cheng, Y.; Prusoff, W. H. Relationship between the Inhibition Constant (K1) and the Concentration of Inhibitor Which Causes 50 per Cent Inhibition (I50) of an Enzymatic Reaction. *Biochem. Pharmacol.* **1973**, *22* (23), 3099−3108.
(48) Vallaster, Bernadette ; Forster, Lisa; Bresinsky, Merlin; Wirth, Lukas; et al. Refinement of Peptidomimetics toward MUR-2425: A Brain-Penetrant and Selective Caspase-2 Inhibitor with Enhanced Pharmacokinetics. *J. Med. Chem.* 2026.

Downloaded from pubs.acs.org/jmcmar/article-pdf/doi/10.1021/acs.jmedchem.6c01370/6911434/jm6c01370.pdf by UNIV REGENSBURG user on 17 November 2026

https://doi.org/10.1021/acs.jmedchem.6c01370
J. Med. Chem. XXXX, XXX, XXX−XXX